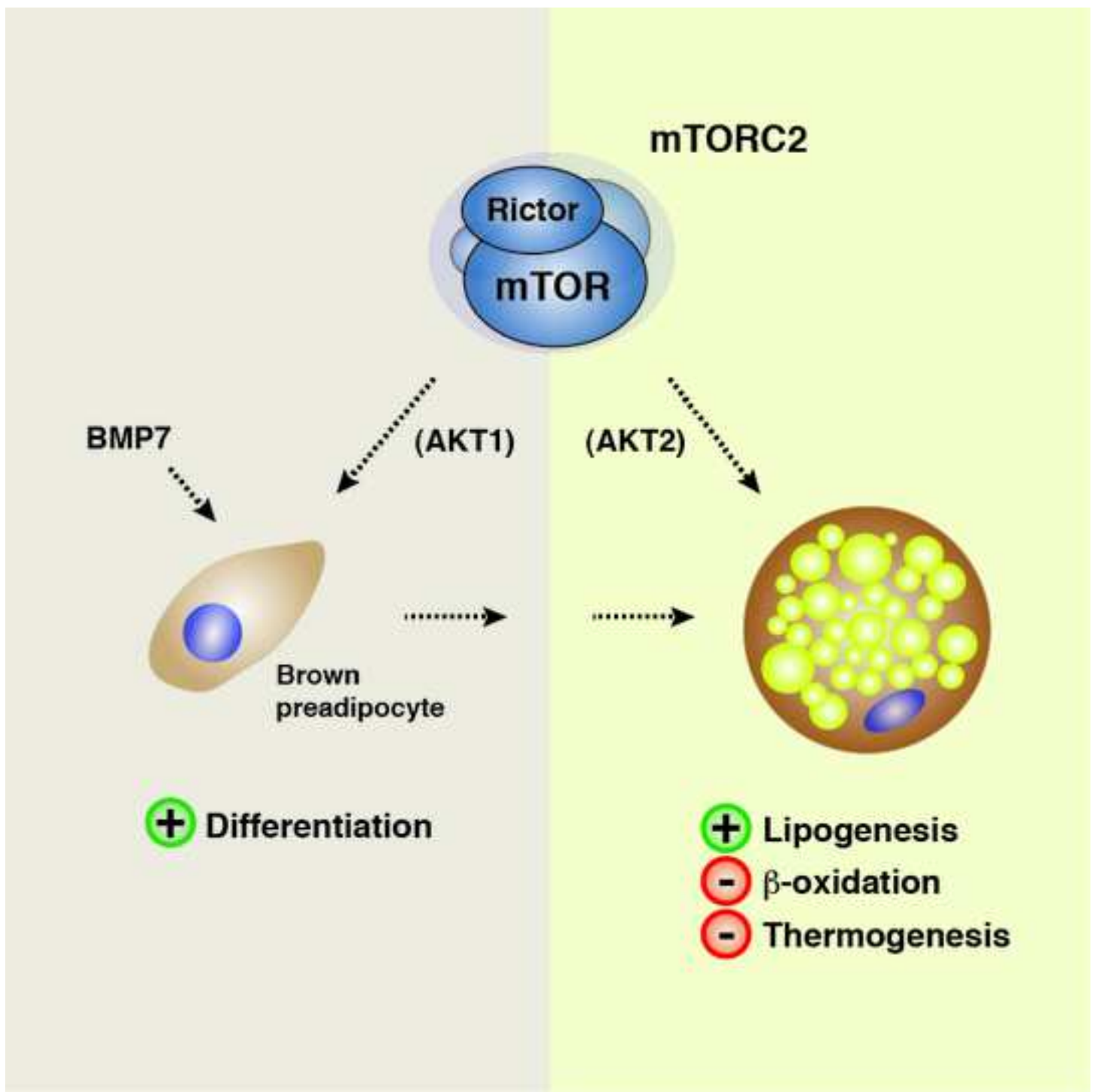




Rictor/mTORC2 Loss in the Myf5 Lineage Reprograms Brown Fat Metabolism and Protects Mice against Obesity and Metabolic Disease

The Harvard community has made this article openly available. [Please share](#) how this access benefits you. Your story matters

| | |
|-------------------|---|
| Citation | Hung, Chien-Min, Camila Martinez Calejman, Joan Sanchez-Gurmaches, Huawei Li, Clary B. Clish, Simone Hettmer, Amy J. Wagers, and David A. Guertin. 2014. "Rictor/mTORC2 Loss in the Myf5 Lineage Reprograms Brown Fat Metabolism and Protects Mice Against Obesity and Metabolic Disease." <i>Cell Reports</i> 8 (1) (July): 256–271. doi:10.1016/j.celrep.2014.06.007. |
| Published Version | doi:10.1016/j.celrep.2014.06.007 |
| Citable link | http://nrs.harvard.edu/urn-3:HUL.InstRepos:25203005 |
| Terms of Use | This article was downloaded from Harvard University's DASH repository, and is made available under the terms and conditions applicable to Open Access Policy Articles, as set forth at http://nrs.harvard.edu/urn-3:HUL.InstRepos:dash.current.terms-of-use#OAP |



HIGHLIGHTS

- Brown and white adipocyte growth requires mTORC2
- mTORC2 promotes lipogenesis and suppresses β -oxidation in brown fat
- Brown preadipocytes also require mTORC2 to differentiate in vitro
- Inhibiting mTORC2 in BAT enhances diet-induced thermogenesis

1 **Rictor/mTORC2 Loss in the *Myf5*-lineage**
2 **Reprograms Brown Fat Metabolism and Protects**
3 **Mice against Obesity and Metabolic Disease**

4

5 Chien-Min Hung¹, Camila Martinez Calejman¹, Joan Sanchez-Gurmaches¹, Huawei Li¹, Clary
6 B. Clish², Simone Hettmer^{3,4,5,7,8}, Amy J. Wagers^{3,4,5,6}, and David A. Guertin^{1*}

7

8 ¹Program in Molecular Medicine, University of Massachusetts Medical School, Worcester,
9 MA 01605, USA

10 ²Broad Institute, Cambridge, Massachusetts, USA 02142

11 ³Howard Hughes Medical Institute

12 ⁴Department of Stem Cell and Regenerative Biology, Harvard Stem Cell Institute, 7 Divinity
13 Avenue, Cambridge, MA 01238, USA

14 ⁵Joslin Diabetes Center, One Joslin Place, Boston, MA 02215, USA

15 ⁶Department of Cell Biology, Harvard Medical School, Boston, MA 02155, USA

16 ⁷Department of Pediatric Oncology, Dana Farber Cancer Institute, Boston, MA 02155

17 ⁸Division of Pediatric Hematology/Oncology, Children's Hospital, Boston, MA 02155

18

19

20 *Correspondence: david.guertin@umassmed.edu

21 Contact Information

22 Phone: 508-856-8065

23 Fax: 508-856-4289

24

25

26

27 **Running Title:** mTORC2 regulates brown adipocyte function

28

29

30

31 **Summary**

32

33 The in vivo functions of mTORC2, and the signaling mechanisms that control brown
34 adipose tissue (BAT) fuel utilization and activity, are not well understood. Here, by
35 conditionally deleting *Rictor* in the *Myf5*-lineage, we provide in vivo evidence that mTORC2
36 is dispensable for skeletal muscle development and regeneration but essential for BAT
37 growth. Furthermore, deleting *Rictor* in *Myf5* precursors shifts BAT metabolism to a more
38 oxidative and less lipogenic state and protects mice from obesity and metabolic disease at
39 thermoneutrality. We additionally find that Rictor is required for brown adipocyte
40 differentiation in vitro, that the mechanism specifically requires AKT1 hydrophobic motif
41 phosphorylation but is independent of pan-AKT signaling, and is rescued with BMP7. Our
42 findings provide new insights into the signaling circuitry that regulates brown adipocytes
43 and could have important implications for developing therapies aimed at increasing energy
44 expenditure as a means to combat human obesity.

45

46

47

48

49 **Introduction**

50

51 Adipose tissue is essential for many biological processes and its dysfunction, for
52 example in obesity, is associated with a growing spectrum of human diseases. Thus,
53 understanding the developmental and metabolic regulation of adipose tissue has broad
54 clinical implications. There are two main classifications of adipose tissue based on
55 histological appearance: white adipose tissue (WAT) and brown adipose tissue (BAT).
56 WAT is the major energy storage site in the body and has critical endocrine functions
57 (Gesta et al., 2007) while BAT dissipates energy as heat in a process called nonshivering
58 thermogenesis (Cannon and Nedergaard, 2004). BAT is particularly important in small
59 rodents and newborn humans to defend against cold exposure and its functional relevance
60 in adult humans was only recently appreciated (Cypess et al., 2009; Nedergaard et al.,
61 2007; van Marken Lichtenbelt et al., 2009; Virtanen et al., 2009). Brown adipocytes are
62 thermogenic because they express Uncoupling Protein 1 (UCP1), which embeds in the
63 inner mitochondrial membrane and produces heat by uncoupling oxidative metabolism
64 from ATP production. The energy expending properties of brown adipocytes coupled with
65 the observation that human BAT amount inversely correlates with body fat mass (Cypess et
66 al., 2009; van Marken Lichtenbelt et al., 2009) is garnering interest in developing strategies
67 to increase brown adipocyte number and/or activity to treat obesity (Harms and Seale,
68 2013; Nedergaard and Cannon, 2010; Tseng et al., 2010). However, the mechanisms—and
69 in particular the signaling circuitry—by which BAT regulates its energy supply and usage
70 are poorly understood (Townsend and Tseng, 2014). With the obesity pandemic
71 seemingly out of control, and with a desperate need for novel therapeutics, the importance
72 of elucidating mechanisms controlling adipocyte growth and function cannot be overstated.

73

74 Studying the in vivo mechanisms that control adipose tissue growth has been
75 challenging because adipocyte origins are not well understood and consequently there are
76 few tools available that are useful for genetically targeting adipocyte precursors in vivo
77 (e.g. by Cre-Lox). Mesenchymal precursors cells expressing *Myf5* give rise to myocytes,
78 brown adipocytes, and a subset of white adipocytes (Sanchez-Gurmaches and Guertin,
79 2014b; Sanchez-Gurmaches et al., 2012; Seale et al., 2008) and several recent studies have

80 successfully used the *Myf5-cre* knock-in allele (Tallquist et al., 2000) to study brown
81 adipose tissue development (Harms et al., 2014; Martinez-Lopez et al., 2013; Ohno et al.,
82 2013; Sanchez-Gurmaches et al., 2012; Schulz et al., 2013). Thus, the multi-fate potential of
83 *Myf5* precursors provides an opportunity to use genetics to distinguish between signaling
84 mechanisms that are required in vivo for the growth of myocytes versus adipocytes.

85

86 The mechanistic target of rapamycin (mTOR) kinase is a master-regulator of growth
87 that functions in at least two distinct complexes called mTORC1 (defined by the Raptor
88 subunit) and mTORC2 (defined by the Rictor subunit) (Laplante and Sabatini, 2012). While
89 much is known about the inputs, outputs, and regulatory features of mTORC1, mTORC2
90 regulation and function remains more enigmatic (Ben-Sahra et al., 2013; Laplante and
91 Sabatini, 2012; Robitaille et al., 2013). The best-described biochemical function of
92 mTORC2 is to phosphorylate the hydrophobic motif (HM) of AKT (S473 in AKT1) and the
93 related SGK (S422 in SGK1) kinases (Garcia-Martinez and Alessi, 2008; Sarbassov et al.,
94 2005). AKT has many effectors including GSK3 β , FoxO1/3, and mTORC1 (through TSC2
95 and PRAS40) and most models indicate mTORC2 is an essential upstream regulator of pan-
96 AKT activity (Laplante and Sabatini, 2012). However, the extent to which this is the case in
97 vivo remains unclear because *Rictor* deficient mouse embryo fibroblasts, which lack
98 mTORC2, have seemingly normal GSK3 β phosphorylation, mTORC1 activity, and only
99 partially decreased FoxO1/3 phosphorylation (Guertin et al., 2006; Jacinto et al., 2006;
100 Shiota et al., 2006).

101

102 Mice lacking *Rictor* die around E10.5 (Guertin et al., 2006; Jacinto et al., 2006; Shiota
103 et al., 2006); therefore, mTORC2 function in vivo is mostly being investigated using floxed
104 *Rictor* alleles. In adipose tissue, two studies using *aP2-cre* to delete *Rictor* reported no
105 effect on individual adipocyte size or overall adipose tissue mass (Cybulski et al., 2009;
106 Kumar et al., 2010). One of the studies finds *aP2-cre;Rictor^{fl/fl}* mice eventually develop mild
107 glucose intolerance and ectopic lipid deposition although a mechanism was not elucidated
108 (Kumar et al., 2010). Notably however, the utility of *aP2-cre* as a tool to target adipocytes
109 has recently been questioned (Lee et al., 2013; Mullican et al., 2013; Wang et al., 2013);

110 therefore, the exact function of mTORC2 in adipose tissue remains unclear. Deleting
111 *Rictor* in skeletal muscle with *Hsa-cre* or *Mck-cre* also has no effect on muscle fiber size or
112 overall muscle mass and only minor effects on insulin-mediated glucose metabolism
113 (Bentzinger et al., 2008; Kumar et al., 2008). The relatively mild phenotypes associated
114 with conditional ablation of *Rictor* in adipose tissue and muscle are somewhat surprising
115 considering the importance of AKT and its downstream effectors in metabolism; however,
116 in both cases (adipose tissue and muscle) the Cre drivers mentioned above reportedly
117 target mature cells and thus the in vivo role of mTORC2 in adipose tissue and muscle
118 precursors is unknown.

119

120 Here, we take advantage of the fact that *Myf5-cre* expresses in precursors of muscle
121 and brown adipocytes to investigate the role of Rictor (i.e. mTORC2) and for comparison
122 Raptor (i.e. mTORC1) in muscle and BAT growth. We report that *Raptor* is essential in the
123 *Myf5* lineage for myogenesis, establishing BAT precursors, and viability. In contrast, *Rictor*
124 is dispensable for myogenesis and viability, but essential for normal BAT growth.
125 Moreover, Rictor-deficient BAT is more metabolically active, having elevated mitochondrial
126 activity, decreased lipogenesis gene expression, and reduced lipid storage. Importantly,
127 deleting *Rictor* in the *Myf5*-lineage also augments diet-induced thermogenesis, which
128 protects mice from an obesogenic diet at thermoneutrality. We also find that *Myf5*-lineage
129 white adipocytes require Rictor for normal growth in vivo suggesting a broader role for
130 mTORC2 in adipose tissue growth. Finally, we show that Rictor is also required in vitro for
131 brown adipocyte differentiation but not for pan-AKT activity, and that this differentiation
132 defect is rescued with BMP7. Collectively, our results provide new insight into the in vivo
133 and in vitro regulation of brown adipocytes and implicate Rictor/mTORC2 as a critical
134 signaling node that regulates the balance between oxidative and lipogenic metabolic states.

135

136

137

138 **Results**

139

140 **Rictor is dispensable in the *Myf5* lineage during embryogenesis**

141

142 Precursors expressing *Myf5* give rise to brown adipocytes, a subset of white
143 adipocytes, and skeletal muscles (Sanchez-Gurmaches and Guertin, 2014a; Sanchez-
144 Gurmaches et al., 2012; Seale et al., 2008). We took advantage of this to investigate the
145 role of mTORC1 versus mTORC2 in vivo in fat versus muscle development by generating
146 *Myf5-cre;Raptor^{fl/fl}* (*Raptor^{Myf5cKO}*) and *Myf5-cre;Rictor^{fl/fl}* (*Rictor^{Myf5cKO}*) conditional
147 knockout mice. The *Rictor^{Myf5cKO}* mice are born at the expected Mendelian ratio and show
148 no obvious motor or behavioral defects [not shown]. In contrast, *Raptor^{Myf5cKO}* mice die
149 perinatally. E16.5 *Raptor^{Myf5cKO}* embryos are smaller due to a muscle development defect
150 that is not apparent in control or *Rictor^{Myf5cKO}* embryos [Figure S1A-D]. For example,
151 transverse sections through the head and neck of *Raptor^{Myf5cKO}* embryos reveal an
152 underdeveloped tongue and the absence of the masseter, sternohyoid, hyoglossus,
153 supraspinatus, prevertebral, and trapezius muscles, the later deficiency resulting in hind
154 neck body wall fragility during specimen preparation [Figure S1A-D]. Thus, *Raptor* is
155 essential in the *Myf5* lineage for viability and muscle development while *Rictor* is
156 dispensable for both.

157

158 To confirm that *Rictor* is dispensable for myogenesis, we purified satellite cells
159 (which express *Myf5*) from *Rictor^{Myf5cKO}* skeletal muscles, confirmed they are deleted for
160 *Rictor* [Figure S1E], and show they differentiate ex vivo into myosin heavy chain-positive
161 multinucleate myofibers [Figure S1F-G]. Moreover, deleting *Raptor* in satellite cells in
162 vivo with Pax7-CreER completely blocks skeletal muscle repair, while deleting *Rictor* by the
163 same approach does not prevent muscle regeneration following acute injury [Figure S1H-I].
164 Thus, *Rictor* is also dispensable for satellite cell differentiation ex vivo and for adult
165 myogenesis induced by injury.

166

167 White adipose tissues develop postpartum in mice, but early brown adipocyte
168 precursor cells (bAPCs) are easily detectable in E16.5 embryos by Hematoxylin and Eosin

169 (H&E) stain. Qualitatively similar pools of cervical, interscapular, and subscapular bAPCs
170 are clearly detectable in control and *Rictor*^{Myf5cKO} E16.5 embryos [Figure S1A & S1D]. In
171 contrast, interscapular and subscapular bAPCs are absent in E16.5 *raptor*^{Myf5cKO} embryos
172 [Figure S1A & S1D]. Notably, a diminished pool of cervical bAPCs is detectable in the
173 *Raptor*^{Myf5cKO} embryos, which is consistent with our lineage tracing data showing that only
174 about half of the cervical brown adipocytes arise from *Myf5-cre* expressing precursors
175 [Figure 1SD](Sanchez-Gurmaches and Guertin, 2014b). Thus, Raptor but not Rictor is also
176 essential in the *Myf5*-lineage for establishing bAPCs during embryogenesis.

177

178 **Brown and white adipose tissue growth requires Rictor**

179

180 Although *Rictor*^{Myf5cKO} mice show no obvious embryonic phenotypes, they tend to
181 weigh less (not significantly) than controls at postnatal day 1 (P1) [Figure S1J], which
182 reaches significance from 6-15 weeks of life [Figure 1A]. Individual tissue analysis
183 indicates that the weight difference results from decreased adipose tissue mass. For
184 example, the interscapular BAT (iBAT) in P1 *Rictor*^{Myf5cKO} neonates weighs about 30% less
185 than normal [Figure S1K] and during the first weeks of life the mutant BAT grows but to a
186 much smaller size, resulting in mutant iBAT and subscapular BAT (sBAT) depots at 6-
187 weeks weighing about 50% less than controls and being darker in color [Figure 1B].
188 Adipocytes in the retroperitoneal and anterior subcutaneous WAT depots (rWAT, asWAT)
189 are also derived largely from *Myf5-cre* expressing precursors (Sanchez-Gurmaches et al.,
190 2012) and both of these depots also decrease in mass by approximately 50% in the
191 *Rictor*^{Myf5cKO} mice [Figure 1C]. In contrast, the posterior subcutaneous and peri-gonadal
192 WAT depots (psWAT, pgWAT), which are composed of *Myf5*-negative lineage adipocytes,
193 do not differ in weight [Figure 1C]. Skeletal muscles (e.g. triceps, quadriceps, and
194 gastrocnemius) and all other lean tissues examined except the kidneys (which are slightly
195 larger) are normal size in the knockout [Figure 1D]. Western analysis for Rictor protein
196 confirms *Rictor* deletion and reduced AKT-S473 phosphorylation in iBAT and muscle and
197 to a lesser extent in rWAT and asWAT, but not in psWAT, pgWAT or liver [Figure 1E].

198

199

200 From 6 weeks to 6 months, the mutant iBAT and sBAT shows no additional growth
201 increase while asWAT and rWAT grow to about half (asWAT) or one third (rWAT) the size
202 of their anatomically matched control tissues [Figure 1F]. In contrast, *Rictor*^{Myf5cKO} psWAT,
203 pgWAT, muscles, and liver grow to their normal size in the same time frame [Figure 1F].
204 Thus, *Rictor*^{Myf5cKO} mice can grow small BAT tissues in the first weeks of life; however, as
205 *Rictor*^{Myf5cKO} mice age the iBAT and sBAT maintain their weight while asWAT and rWAT
206 grow at a reduced rate. Collectively, these results indicate Rictor is essential in the *Myf5*
207 lineage for adipose tissue growth but not for skeletal muscle growth.

208

209 **Brown adipocytes lacking Rictor are smaller**

210

211 To better define the BAT growth defect we histologically examined iBAT in control
212 and *Rictor*^{Myf5cKO} mice. At E18.5 there is no qualitative difference between control and
213 *Rictor*^{Myf5cKO} bAPCs pools [Figure 2A]. In P1 neonates however, lipids begin accumulating
214 in control BAT but not in the *Rictor*^{Myf5cKO} BAT [Figure 2A]. From P1 to 6 months lipid
215 droplets grow in size in control BAT but remain small in the *Rictor*^{Myf5cKO} BAT [Figure 2A]
216 resulting in smaller cells measured by the increase in nuclei per mm² [Figure S2A]. Total
217 genomic DNA content (an indirect measure of cell number) is also lower in the *Rictor*^{Myf5cKO}
218 BAT indicating additional tissue hypoplasia [Figure S2B]. In contrast, *Rictor*^{Myf5cKO} skeletal
219 muscle fibers appear histologically identical to control fibers [Figure S2C] consistent with
220 Rictor being dispensable for myocyte growth.

221

222 **Myf5-lineage white adipocytes lacking Rictor are also small and multilocular**

223

224 Compared to controls, many of the adipocytes in the *Rictor*^{Myf5cKO} rWAT and asWAT
225 are also smaller and multilocular [Figure 2B] but the pattern is heterogeneous in that
226 several large unilocular white adipocytes are also detectable. The appearance of psWAT
227 and pgWAT adipocytes is unchanged in the knockout [Figure S2C]. We recently discovered
228 that the adipocyte precursor pools in rWAT and asWAT are a mix of *Myf5-cre* lineage
229 positive and negative precursors (Sanchez-Gurmaches et al., 2012). Therefore, we
230 reasoned that the size heterogeneity in *Rictor*^{Myf5cKO} rWAT and asWAT could reflect a

231 mosaic of *Myf5*-lineage negative (i.e. undeleted) and *Myf5*-lineage positive (i.e. *Rictor*
232 knockout) cells. To test this we incorporated the *Rosa26-mTmG* reporter (Muzumdar et al.,
233 2007) into control and *Rictor^{Myf5cKO}* mice to irreversibly label Cre-expressing cells and their
234 lineages with membrane-targeted eGFP (mGFP); all other (Cre^{neg}) cells and their
235 descendants are labeled with membrane targeted tdTomato fluorescent protein (mTFP).
236 The result is unequivocal; only the small adipocytes are mGFP⁺ in *Rictor^{Myf5cKO}* rWAT and
237 asWAT while all the large unilocular adipocytes are mTFP⁺ [Figure 2C]. As expected, in
238 both the control and *Rictor^{Myf5cKO}* mice the iBAT adipocytes are mGFP⁺ and the psWAT and
239 pgWAT adipocytes are mTFP⁺ [Figure S2D]. We examined UCP1 expression by
240 immunohistochemistry in the asWAT and rWAT and detect a slight increase in UCP1
241 staining in the *Rictor^{Myf5cKO}* adipocytes suggesting the cells might have brown-adipocyte like
242 characteristics [Figure S2E] (not shown). Nevertheless, these data confirm that the
243 heterogeneous small cell phenotype in the *Myf5*-lineage white adipocytes is the result of
244 cell-autonomous *Rictor* deletion.

245

246 **Lipogenesis is decreased in Rictor-deficient BAT**

247

248 We hypothesized that the paucity of lipid and marked color difference between
249 control and *Rictor^{Myf5cKO}* BAT indicates a metabolic shift to a more oxidative state. To test
250 this we first examined AKT signaling in BAT, which positively regulates lipogenesis. In vivo
251 PDK1-mediated AKT-T308 phosphorylation is intact in both fasted/re-fed and insulin-
252 stimulated *Rictor^{Myf5cKO}* BAT despite ablation of phospho-AKT S473 and phospho-AKT T450
253 (which is also mTORC2 dependent) [Figure 3A & S3A], consistent with the ability of T-loop
254 (T308) and hydrophobic motif (S473) phosphorylation to be regulated independently
255 (Pearce et al., 2010). Surprisingly, phosphorylation of the classic AKT substrates FoxO1/3,
256 GSK3 β , TSC2, PRAS40, and AS160 is normal in *Rictor^{Myf5cKO}* BAT [Figure 3A] indicating that
257 Rictor is not essential in BAT for pan-AKT signaling. Rictor loss in BAT also does not affect
258 phosphorylation of the SGK substrate NDRG1 [Figure 3A] indicating mTORC2 is also not
259 essential in BAT for SGK signaling to NDRG1 or that a compensatory pathway exists.

260

261 Next we examined whether deleting *Rictor* in the *Myf5*-lineage affects expression of
262 BAT differentiation markers. In P1 neonates, *Prdm16*, *C/ebp α* , and *C/ebp β* expression do
263 not significantly differ between controls and knockouts, while *Ppar γ* and *Ucp1* levels
264 slightly decrease [Figure 3B] indicating a possible delay in BAT maturation in the
265 knockouts. However, by 6 weeks *Ppar γ* , *Prdm16*, and *C/ebp α* all express at control levels
266 while *C/ebp β* , *Ucp1*, and *Dio2* express at significantly higher than control levels [Figure 3B].
267 The mature adipocyte markers *Cidea* and *aP2* are unchanged between control and
268 knockout both at P1 and 6 weeks [Figure 3B]. Consistent with the gene expression data,
269 PPAR γ , UCP1, and insulin receptor beta (IR β) proteins also express at near control levels in
270 *Rictor^{Myf5cKO}* BAT [Figure 3A]. Thus, while brown adipocyte maturation may be slightly
271 delayed in late embryonic or early neonatal development, terminal differentiation per se
272 (i.e. PPAR γ , UCP1, and IR β induction) occurs in *Rictor^{Myf5cKO}* brown adipocytes and if
273 anything, the *Rictor^{Myf5cKO}* BAT exhibits a stronger “brown” signature.

274
275 Next we examined lipogenesis genes. In P1 *Rictor^{Myf5cKO}* BAT, acetyl-coA
276 carboxylase (*Acc*), fatty acid synthase (*Fasn*), and fatty acid elongase 6 (*Elovl6*) decrease
277 expression by (40%), (40%), and (25%) respectively [Figure 3C]. By 6 weeks, expression
278 of ATP citrate lyase (*Acly*) in addition to *Acc*, *Fasn*, and *Elovl6* is reduced by 90%, 75%, 80%,
279 and 40% respectively [Figure 3C], which we confirmed by Western blot for ACLY and ACC
280 [Figure 3A]. In addition, stearoyl-CoA desaturase (*Scd1*) decreases expression by 45% in 6
281 week *Rictor^{Myf5cKO}* BAT [Figure 3C]. The SREBP1c and ChREBP transcription factors
282 regulate lipogenesis gene expression (Czech et al., 2013; Filhoulaud et al., 2013). In both
283 P1 and 6-week *Rictor^{Myf5cKO}* BAT, the mRNA expression of SREBP1c (*Sreb1c*), which is
284 induced by insulin, and ChREBP (α and β isoforms), which is induced by glucose, is similar
285 [Figure 3D]. However, there is a marked decrease in the amount nuclear SREBP1c
286 (nSREBP1c), the transcriptionally active SREBP1c cleavage product, in the *Rictor*-deficient
287 BAT [Figure 3A] consistent with the decrease in lipogenic gene expression. The levels of
288 *insig1*, another nSREBP1c target gene and negative regulator of SREBP1c processing, also
289 decreases [Figure 3C]. The mRNA expression of SREBP2 (which regulates cholesterol
290 biosynthesis) slightly decreases in *Rictor^{Myf5cKO}* BAT at 6 weeks, but the SREBP2 target

291 genes HMG-CoA synthase (*Hmg-cs*) and HMG-CoA reductase (*Hmg-cr*) express at similar
292 levels in control and knockout BAT [Figure 3D] and nuclear SREBP2 protein (nSREBP2)
293 accumulates possibly to even higher levels in the knockout BAT [Figure 3A]. The post-
294 translational regulation of ChREBP is poorly understood and therefore we could not
295 determine if ChREBP protein function is normal. We also find no difference in AMPK
296 phosphorylation (which is a negative regulator of lipogenesis) between control and
297 *Rictor^{Myf5cKO}* BAT [Figure 3A] or in hormone sensitive lipase (HSL) phosphorylation [Figure
298 S3A]. Together, these results indicate that despite having seemingly normal AKT signaling,
299 de novo lipogenesis is dramatically reduced in *Rictor^{Myf5cKO}* BAT.

300

301 **Mitochondrial activity is elevated in Rictor-deficient BAT**

302

303 To further examine the metabolic state of *Rictor^{Myf5cKO}* BAT we next examined
304 mitochondrial activity. In P1 neonate *Rictor^{Myf5cKO}* BAT, *Pgc1a* expresses normally, while
305 expression of mitochondrial transcription factor A (*Tfam*), which regulates mtDNA
306 replication, and carnitine palmitoyltransferase 1B (*Cpt1b*), which encodes the rate-limiting
307 enzyme in beta-oxidation, slightly decreases [Figure 4A]. Thus, increased mitochondrial
308 activity does not appear to accompany the lipogenesis defect in P1 *Rictor^{Myf5cKO}* neonates.
309 In contrast, *Pgc1a*, *Tfam*, and *Cpt1b* in addition to *Ucp1* express at significantly higher levels
310 in the BAT of 6-week old *Rictor^{Myf5cKO}* mice [Figure 4A & 3B] suggesting overall BAT
311 mitochondrial activity progressively increases in the *Rictor^{Myf5cKO}* mice as they age.

312

313 To explore this in more detail, we used qRT-PCR arrays to broadly measure
314 mitochondrial gene expression in the 6-week old BAT. Using arrays for functional genes
315 involved in mitochondrial molecular transport and biogenesis (including *Ucp1* and *Cpt1b*),
316 we detect significant increases in several genes in addition to *Ucp1* and *Cpt1b* that indicate
317 increased mitochondrial activity [Figure 4B]. Furthermore, the mitochondrial citrate and
318 malate transporters *Slc25a1* and *Slc25a10* respectively—both of which function in fatty
319 acid biosynthesis, the former also being an SREBP1c target gene (Infantino et al., 2007;
320 Mizuarai et al., 2005)—significantly decrease expression in the mutant BAT. Using
321 mitochondrial energy metabolism gene arrays, we found 58 additional genes involved in

322 respiration to also be significantly elevated in *Rictor^{Myf5cKO}* BAT relative to controls [Figure
323 S4A] suggesting an increase in overall mitochondrial mass, which we confirmed by
324 immunofluorescence staining with CoxIV [Figure 4C]. Transmission electron microscopy
325 (TEM) further reveals individual mitochondria in the mutant BAT are morphologically
326 larger and have more disorganized cristae [Figure 4D]. To directly confirm that
327 mitochondrial activity is elevated, we measured the oxygen consumption rate (OCR) of
328 control and *Rictor^{Myf5cKO}* BAT in a Seahorse Flux Analyzer and determined that both basal
329 and pyruvate-stimulated OCR are elevated by around 18% in *Rictor^{Myf5cKO}* BAT [Figure 4E].
330 We did not detect a significant increase in overall oxygen consumption when *Rictor^{Myf5cKO}*
331 mice were placed in metabolic cages at 22°C except when normalized for body weight
332 [Figure S4B]. Notably however, mice are under thermal stress at this temperature, which
333 can mask effects on BAT activity (Feldmann et al., 2009).

334
335 Interestingly, we also detect an approximate 2-fold increase in basal glucose uptake
336 in *Rictor^{Myf5cKO}* BAT measured by ¹⁸F-DG-PET CT scanning [Figure S4C] and a significant
337 increase in lipoprotein lipase (*Lpl*) expression [Figure 3C] suggesting that *Rictor^{Myf5cKO}* BAT
338 may consume more nutrients than age matched control BAT. Small metabolite profiling
339 reveals that *Rictor^{Myf5cKO}* BAT also has elevated levels of inosine monophosphate (IMP)
340 [Figure S4D], a deamination product of adenosine monophosphate (AMP), the
341 accumulation of which suggests increased uncoupling (Balcke et al., 2011). In an acute cold
342 challenge *Rictor*-deficient BAT also induces *Ucp1* expression significantly more than
343 control BAT and the mutants have no difficulty maintaining body temperature, although
344 notably body temperature regulation in an acute cold challenge is largely a function of
345 muscle [Figure 4F]. Finally, we see no compensatory “browning” in the psWAT as would be
346 expected if *Rictor^{Myf5cKO}* BAT were dysfunctional [Figure S2C-D](Schulz et al., 2013). These
347 results are consistent with *Rictor* loss in BAT shifting metabolism to a more oxidative and
348 less lipogenic state.

349
350 **Brown preadipocytes require *Rictor* to differentiate in vitro**

351

352 To examine if the brown adipocyte differentiation program also requires Rictor in
353 vitro, we generated brown adipocyte precursor cells (bAPCs) harboring an inducible
354 knockout system (i.e. *Rictor^{iKO}*) in which *Rictor* deletion is triggered by 4-hydroxytamoxifen
355 (4-OHT) [Figure S5A]. The advantage of this approach is that acute *Rictor* loss can be
356 compared to isogenic controls. Inducibly deleting *Rictor* rapidly and robustly depletes
357 Rictor protein and AKT-S473 phosphorylation, and consistent with our in vivo data, leaves
358 AKT-T308 phosphorylation intact [Figure S5B]. Also consistent with the in vivo results,
359 both basal and insulin-stimulated phosphorylation of FoxO1/3, GSK3 β , TSC2, and PRAS40
360 are normal in *Rictor^{iKO}* bAPCs [Figure 5A]. S6K1 phosphorylation is also unaffected [Figure
361 5A]. Contrary to the in vivo results, acute *Rictor* loss in vitro decreases phosphorylation of
362 the SGK target NDRG1 [Figure 5A]. This indicates Rictor is required in cultured bAPCs for
363 SGK activity to NDRG1 but not for pan-AKT or mTORC1 activity.

364
365 To our surprise, *Rictor^{iKO}* bAPCs are completely incapable of synthesizing lipid
366 droplets in vitro when induced to differentiate [Figure 5B]. This is surprising because
367 *Rictor^{iKO}* cells maintain normal levels of AKT-T308, GSK3 β -S9, and S6K1-T389
368 phosphorylation (i.e. PDK1, AKT, and mTORC1 activity respectively) throughout the
369 differentiation protocol [Figure 5C]. The differentiation block occurs early as *Rictor^{iKO}*
370 bAPCs fail to induce *C/ebp α* , *Ppar γ* , *Prdm16*, *Pgc1 α* , *Srebf1c*, *Ucp1*, and *Glut4* [Figure 5D &
371 S5C]. The expression of *C/ebp δ* and *C/ebp β* on the other hand induces normally and
372 slightly higher in the *Rictor^{iKO}* bAPCs respectively at differentiation day 6 [Figure 5D].
373 Consistent with the gene expression data, PPAR γ , IR β , UCP1, nSREBP1c, ACC, and ACLY
374 levels fail to increase during differentiation in *Rictor^{iKO}* bAPCs [Figure 5E]. Notably, 4-OHT
375 or CreER activation alone (i.e. in the absence of *Rictor* floxed alleles) has no effect on
376 differentiation [not shown]. Moreover, bAPCs prepared from P1 *Rictor^{Myf5cKO}* neonates also
377 fail to differentiate in vitro indicating that the ex vivo differentiation block is not unique to
378 using the inducible knockout-system [Figure S5D]. Importantly, expressing recombinant
379 PPAR γ in *Rictor^{iKO}* bAPCs rescues IR β , UCP1 and nSREBP1c expression [Figure 5F] and lipid
380 droplet production [Figure 5G] in the absence of Rictor indicating that Rictor promotes
381 bAPC differentiation at least in part by facilitating PPAR γ induction.

382

383 *Insulin receptor substrate 1 (Irs1)* and *Irs3* knockout bAPCs also fail to induce PPAR γ
384 ex vivo (Fasshauer et al., 2001). It was later shown that *Irs1/3* KO bAPCs are unable to
385 differentiate because they express high levels of *Pref-1*, *Wnt10a*, and *Necdin*, which encode
386 adipogenesis inhibitors (Tseng et al., 2005). In contrast, *Rictor*-deficient bAPCs express
387 normal levels of *Pref-1*, *Wnt10a*, and *Necdin* in culture, and during differentiation *Necdin*
388 and *Pref-1* increase but only late in the differentiation protocol [Figure S5C]. Thus, the
389 mechanism by which deleting *Rictor* inhibits brown adipocyte differentiation differs from
390 that of deleting *Irs1/3*.

391

392 **AKT1 functions downstream of Rictor in brown adipocyte differentiation**

393

394 To further explore the mechanism by which Rictor regulates brown adipocyte
395 differentiation, we next asked whether an AKT or SGK pathway is required downstream of
396 Rictor for differentiation in vitro. To this end, we generated *Rictor^{iKO}* bAPCs that express
397 HA-SGK1, HA-AKT1, HA-AKT2, or their phosphomimetic counterparts HA-SGK-S422D, HA-
398 AKT1-S473D, HA-AKT2-S474D in which a phosphomimetic residue was placed at the
399 mTORC2 hydrophobic motif site, and asked whether any of these constructs rescue
400 differentiation. Only HA-AKT1-S473D efficiently rescues lipid biosynthesis [Figure 6A].
401 HA-AKT1-S473D-expressing *Rictor^{iKO}* bAPCs also induce PPAR γ to control levels, and
402 consequently, IR β , UCP1, nSREBP1c, ACLY, and ACC expression are all restored [Figure 6B].
403 We confirmed that all of the recombinant proteins are functional [Figure S6A]. Thus, Rictor
404 promotes differentiation as part of mTORC2 and through an AKT pathway, not an SGK
405 pathway.

406

407 Our rescue experiments point to AKT1 as the specific isoform driving bAPC
408 differentiation in vitro. Consistent with this notion, AKT1 is more highly expressed in
409 undifferentiated precursors and decreases expression during differentiation while AKT2
410 expresses at lower levels in undifferentiated precursors and induces late during
411 differentiation [Figure S6B]. To further examine the role of AKT1 and AKT2 in bAPC
412 differentiation, we created *Myf5-cre;Akt1^{flxed}* and *Myf5-cre;Akt2^{flxed}* mice and from them

413 generated bAPC lines that specifically lack either *Akt1* or *Akt2* and determined their vitro
414 differentiation capacity. Consistent with AKT1 but not AKT2 being more essential for
415 differentiation, *Akt1*-deficient bAPCs cannot efficiently synthesize lipid droplets [Figure
416 S6C] or up-regulate PPAR γ , IR β , or UCP1 when induced to differentiate [Figure S6D]. In
417 contrast, *Akt2*-deficient bAPCs induce PPAR γ , IR β , and UCP1 to control levels [Figure S6C]
418 indicating that AKT1 is indeed the isoform required downstream of Rictor/mTORC2 for
419 brown adipocyte differentiation.

420

421 **BMP7 rescues brown adipocyte differentiation in the absence of Rictor**

422

423 Our in vitro studies uncovered a paradoxical relationship between our in vivo and in
424 vitro models; in vitro *Rictor^{iKO}* bAPCs cannot differentiate (i.e. induce PPAR γ and UCP1), but
425 in vivo Rictor-deficient BAT clearly develops and is positive for both PPAR γ and UCP1. We
426 had first hypothesized that in vitro bAPCs might require SGK activity to differentiate
427 because SGK activity is decreased in vitro but not in vivo in the absence of Rictor; however,
428 our rescue experiments with recombinant phosphomimetics argue against this. An
429 alternative hypothesis is that in vivo, in the natural environment, there are developmental
430 signals present that are missing from the artificial in vitro differentiation assay. The signals
431 that drive brown adipocyte differentiation in vivo are poorly understood. One proposed
432 inducer of brown adipocyte differentiation is the transforming growth factor- β superfamily
433 member BMP7 [Schulz and Tseng, 2013; Tseng et al., 2008]. When given to control or
434 *Rictor^{iKO}* bAPCs, BMP7 does not induce AKT phosphorylation [Figure 6C]. However, when
435 supplemented into the differentiation cocktail BMP7 restores to *Rictor^{iKO}* bAPCs their
436 ability to synthesize lipid droplets [Figure 6D] and express PPAR γ , IR β , UCP1 and to a lesser
437 extent nSREBP1c, ACLY, and ACC [Figure 6E]. These results are consistent with the in vitro
438 differentiation assay lacking key signaling molecules present in vivo and suggest that BMP7
439 signaling converges with Rictor/mTORC2-AKT1 signaling on a downstream effector during
440 brown adipocyte differentiation.

441

442 Interestingly, in our in vitro differentiation assays with *Akt1* and *Akt2* deficient
443 bAPCs, we noticed that while the *Akt2*-deficient cells differentiate, they fail to induce
444 nSREBP1C and consistently ACLY and ACC express at low levels [Figure S6D]. This
445 suggests that while AKT2 is not essential for brown adipocyte differentiation, it is
446 important downstream of Rictor/mTORC2 for regulating lipid metabolism in mature
447 brown adipocytes. Consistent with this idea, when we immunoprecipitate AKT1 or AKT2
448 from undifferentiated control and *Rictor^{iKO}* bAPCs, all of the detectable AKT
449 phosphorylation is on AKT1 while in vivo the bulk of AKT phosphorylation appears to shift
450 to AKT2 [Figure S6E-F]. Thus, while the inability of *Rictor^{iKO}* bAPCs to differentiate in
451 culture in the absence of BMP7 reflects an AKT1 pathway deficiency, the in vivo metabolic
452 phenotype appears to reflect an AKT2 pathway deficiency.

453

454 ***Rictor^{Myf5cKO}* mice are less susceptible to obesity and metabolic disease at** 455 **thermoneutrality**

456

457 The higher metabolic activity of Rictor-deficient BAT led us to wonder whether
458 *Rictor^{Myf5cKO}* mice are resistant to obesity. Chronic consumption of high fat diet (HFD)
459 triggers a phenomenon in mice called diet-induced thermogenesis, which requires UCP1,
460 and counteracts obesity (Cannon and Nedergaard, 2010; Feldmann et al., 2009). Because
461 BAT activity is masked by chronic thermal stress at 22°C (the temperature of our mouse
462 facility), we conducted the following studies at thermoneutrality (30°C for mice), which
463 exempts mice from this thermal stress (Feldmann et al., 2009). When living at 30°C and
464 eating a normal chow diet (chow), control and *Rictor^{Myf5cKO}* mice gain roughly the same
465 amount of weight [Figure 7A] and consume the same amount of total energy [Figure 7B]
466 over a 12-week span. In contrast, when living at 30°C and eating a HFD (45% calories
467 from fat), control mice gain on average 14.67 ± 1.054 grams of weight while *Rictor^{Myf5cKO}*
468 mice only gain 10.570 ± 1.178 grams [Figure 7A] despite both groups again consuming the
469 same amount of total energy [Figure 7B]. This translates into the control cohort gaining
470 64% more weight when eating HFD versus chow than the *Rictor^{Myf5cKO}* mice and suggests
471 the *Rictor^{Myf5cKO}* mice living at thermoneutrality and eating a HFD are less metabolically
472 efficient than controls, which is indeed the case [Figure 7C].

473

474 The resistance to weight gain in the HFD-fed *Rictor^{Myf5cKO}* cohort is partly due to
475 reduced growth of adipose tissue. For example, the pgWAT (the largest white fat depot)
476 gains significantly less mass in the HFD-fed *Rictor^{Myf5cKO}* cohort than in HFD-fed controls
477 [Figure 7D]. The liver and heart also grow larger in the control cohort eating HFD
478 compared to the control cohort eating chow, while the liver and heart grow to the same
479 mass in the *Rictor^{Myf5cKO}* cohorts regardless of the diet [Figure 7D & S7A]. Diet also has no
480 effect on the growth of other lean tissues including skeletal muscles (quadriceps and
481 gastrocnemius), kidney, or pancreas in either the controls or *Rictor^{Myf5cKO}* cohorts [Figure
482 7D & S7A]. That pgWAT grows less in HFD-fed *Rictor^{Myf5cKO}* mice compared to chow-fed
483 controls indicates systemic protection against obesity is occurring because *Myf5*-Cre does
484 not target pgWAT [Figure 1F & S2C]. The reduction in pgWAT mass is due at least in part
485 to smaller adipocyte size [Figure 7E]; the livers of *Rictor^{Myf5cKO}* mice are also resistant to
486 developing hepatic steatosis [Figure 7E]; and the HFD-fed *Rictor^{Myf5cKO}* mice perform better
487 in a glucose tolerance test [Figure S7B], all consistent with systemic protection from
488 obesity.

489

490 In the chow-fed cohorts living without thermal stress, histology reveals that control
491 BAT adopts a more “white adipocyte-like” appearance—that is the lipid droplets appear
492 larger and unilocular [Figure 7E]. In contrast, the BAT in chow-fed *Rictor^{Myf5cKO}* mice
493 resists the whitening effects of living at thermoneutrality and maintains more of a “brown-
494 adipocyte-like” appearance [Figure 7E]. This resistance to whitening is reflected in the
495 gene expression signature using recently identified BAT and WAT identity genes (Harms et
496 al., 2014; Walden et al., 2011); for example, when normalized to BAT gene expression at
497 22°C, the shift to thermoneutrality decreases the expression of BAT-selective genes
498 (*Prdm16*, *Sgk2*, *cideb*, *cyp2b10*) and increases the expression of WAT-selective genes (*Dpt1*,
499 *Retn*, *Trim14*, *Nnmt*) to a greater extent in control BAT than in *Rictor^{Myf5cKO}* BAT, which
500 maintains a more BAT-like identity. [Figure S7C]. Thus, the BAT of *Rictor^{Myf5cKO}* mice
501 consuming chow is resistant to the whitening effects of removing thermal stress.

502

503 In the HFD-fed cohorts living without thermal stress, histology reveals a large
504 number of multi-locular adipocytes in the control BAT [Figure 7F] that are not apparent in
505 the chow-fed controls [Figure 7E] suggesting diet-induced thermogenesis. This is also
506 reflected in the gene expression data as *Prdm16* levels increase in control BAT in HFD-fed
507 mice compared to chow-fed [Figure 7G], while the WAT-specific genes *Retn*, *Trim14*, and
508 *Nnmt* decrease [Figure 7G]. The histology also reveals that *Rictor^{Myf5cKO}* BAT is even more
509 “brown-like” in the HFD-fed cohort exhibiting a uniform abundance of small lipid droplets
510 [Figure 7F] and a stronger BAT-identity gene signature (i.e. elevated *Prdm16*, *Sgk2*, *Cideb*,
511 *Cyp2b10*; decreased *Dpt1*, *Retn*, *Trim14*, *Nnmt*) [Figure 7G]. Consistent with the *Rictor*-
512 deficient BAT being more stimulated by HFD, BAT functional genes (*Ucp1*, *Pgc1α*, *Cpt1β*,
513 *Dio2*) induce to a greater extent in the BAT of HFD-fed *Rictor^{Myf5cKO}* mice [Figure 7H], which
514 maintain relatively low levels of *Acly*, *Acc*, and *Fasn* expression [Figure S7D]. Consistently,
515 UCP1 protein level is higher in the BAT of *Rictor^{Myf5cKO}* mice eating HFD [Figure 7I].
516 Interestingly, after 20 weeks of eating a HFD, the control BAT eventually reverts back to a
517 more “white-adipocyte-like” histology; however, BAT character is preserved in the
518 *Rictor^{Myf5cKO}* mice [Figure S7E]. Collectively, these results suggest that inhibiting mTORC2
519 in BAT increases diet-induced thermogenesis and consequently, *Rictor^{Myf5cKO}* mice living
520 without thermal stress and consuming an obesogenic diet are less susceptible to
521 developing obesity and metabolic disease.

522
523
524

525 **DISCUSSION**

526

527 While transcriptional regulation of BAT development and function has been
528 extensively described (Cristancho and Lazar, 2011; Kajimura et al., 2010), much less is
529 known about the signaling mechanisms that regulate BAT. The control of brown fat fuel
530 utilization is also incompletely understood (Townsend and Tseng, 2014). Previous studies
531 reported that conditionally deleting *Rictor* in white and brown adipose tissue or skeletal
532 muscle has no affect on WAT or BAT mass or individual adipocyte or myocyte size
533 (Bentzinger et al., 2008; Cybulski et al., 2009; Kumar et al., 2008; Kumar et al., 2010).
534 However, these studies used Cre drivers that reportedly delete *Rictor* in mature cells, which
535 led us to hypothesize that Rictor/mTORC2 may be more important in vivo for brown/white
536 adipose tissue and/or muscle development. By conditionally deleting *Rictor* in *Myf5*
537 precursors, which give rise to brown adipocytes, a subset of white adipocytes, and
538 myocytes (Sanchez-Gurmaches and Guertin, 2014b; Sanchez-Gurmaches et al., 2012; Seale
539 et al., 2008) we discovered that Rictor is not essential in vivo for muscle development or
540 regeneration. In contrast, *Myf5*-lineage brown and white adipocytes lacking Rictor are
541 reduced in size. Furthermore, Rictor-deficient BAT undergoes a metabolic shift to a more
542 oxidative and less lipogenic metabolic, despite having normal pan-AKT signaling.
543 Importantly, at thermoneutrality this protects mice against an obesogenic diet. These
544 findings implicate Rictor/mTORC2 as an essential signaling node in BAT that regulates the
545 balance between fatty acid oxidation and storage. Considering that active BAT is now
546 recognized to exist in adult humans, our findings could have important implications for
547 understanding the signaling mechanisms that regulate fuel usage and metabolic activity in
548 human BAT.

549

550 We also report that in vitro brown adipocyte differentiation requires
551 Rictor/mTORC2. Mechanistically, Rictor/mTORC2 promotes *Ppar γ* induction through
552 AKT1 independently of pan-AKT signaling and mTORC1 activity. In vivo however, brown
553 adipocytes differentiate in *Rictor^{Myf5cKO}* mice despite lacking Rictor expression. We
554 hypothesize that this paradox indicates that the artificial in vitro culture conditions lack an

555 important signal present in vivo that can overcome this deficiency. Supporting this notion,
556 supplementing the differentiation assay with BMP7, a proposed in vivo inducer of brown
557 adipocyte differentiation and thermogenesis (Schulz and Tseng, 2013; Tseng et al., 2008),
558 rescues differentiation in the absence of Rictor. Notably, we do in fact detect low *ppar γ*
559 expression in *Rictor^{Myf5cKO}* P1 BAT, which may reflect the role of Rictor/mTORC2 in early
560 brown adipocyte differentiation and explain the mutant BAT hypoplasia. Exactly how
561 Rictor/mTORC2 and BMP7 signaling might converge on PPAR γ is not yet clear. We also
562 show that during brown adipocyte differentiation, the major AKT isoform switches from
563 AKT1 to AKT2; thus, while Rictor/mTORC2 may regulate differentiation through an AKT1
564 pathway that can be bypassed in vivo, its role in BAT metabolism is likely mediated
565 through an AKT2 pathway that cannot be compensated for. Consistent with this idea,
566 whole body *akt2* knockout mice among many other phenotypes have smaller BATs (Cho et
567 al., 2001; Garofalo et al., 2003).

568
569 An unexpected finding in our study is that all of the classic AKT substrates we
570 examined, whether in vitro in *Rictor*-deficient bAPCs or in vivo in mature *Rictor*-deficient
571 brown adipocytes, are phosphorylated normally. Why then does deleting *Rictor* in BAT
572 cause a metabolic shift? One possibility is that forkhead box O (FOXO) transcription factors
573 are more active in *Rictor*-deficient brown adipocytes. FOXOs are regulated by multiple
574 signals and function as cellular homeostasis regulators under stressful conditions
575 (Eijkelenboom and Burgering, 2013). FoxO1 and FoxO3 are classic AKT substrates
576 inhibited by AKT phosphorylation (through 14-3-3 mediated cytoplasmic retention) that
577 are partially dephosphorylated in some *Rictor*-deficient cell types (Guertin et al., 2009;
578 Guertin et al., 2006; Hagiwara et al., 2012; Jacinto et al., 2006; Yuan et al., 2012). When
579 FoxO1 and FoxO3 are dephosphorylated, they translocate to the nucleus where, through
580 poorly understood mechanisms operating in a cell-type specific manners, they affect
581 metabolism, survival, and cell cycle genes (including *Ucp1*) and the activity of
582 transcriptional regulators (including PPAR γ and C/EBP α) (Eijkelenboom and Burgering,
583 2013; Ortega-Molina et al., 2012). However, FoxO1/3 phosphorylation is not affected in
584 *Rictor*-deficient BAT; thus, if the metabolic shift is driven by FOXOs, it may be through an

585 alterative mechanism such as acetylation (Banks et al., 2011; Masui et al., 2013). Another
586 possibility is that FoxC2 mediates the metabolic shift (Cederberg et al., 2001; Yao et al.,
587 2013); however, we do not observe any change in FoxC2 expression in *Rictor*-deficient
588 preadipocytes (not shown), nor do we see effects on the FoxC2 targets *C/ebpβ* or *Wnt10b*
589 during differentiation (Gerin et al., 2009). The most interesting possibility is that the shift
590 is mediated through an unidentified AKT pathway. Whatever the reason, why it differs
591 from other AKT pathways and uniquely requires hydrophobic motif phosphorylation is not
592 clear. This is an important ongoing area of investigation.

593

594 Consistent with the *Myf5*-lineage giving rise to a subset of white adipocytes, we also
595 uncovered an essential role for Rictor/mTORC2 in vivo in white adipocyte growth. This
596 confirms our previous discovery that some white adipocytes arise from *Myf5-cre*
597 expressing precursors (Sanchez-Gurmaches and Guertin, 2014b; Sanchez-Gurmaches et al.,
598 2012). However, because in the *Rictor^{Myf5ckO}* mice the Rictor-deficient white adipocytes are
599 interspersed heterogeneously with non-deleted adipocytes within the same depot, we
600 could not perform the appropriate whole-tissue biochemical studies using Rictor-deficient
601 WAT. We did however determine that *Rictor^{iKO}* white adipocyte precursors purified from
602 the stromal vascular fraction of psWAT (which are not *Myf5*-lineage derived) are also
603 defective at differentiating in vitro (not shown) indicating Rictor also has a cell
604 autonomous role in white adipocyte differentiation that is not dependent upon being *Myf5*-
605 lineage derived. To determine the in vivo relevance of these findings we will need to
606 identify Cre drivers that express uniformly and specifically in white adipocyte precursors;
607 however, the origins of adipocytes are just beginning to be revealed and appropriate tools
608 are not yet available for this line of investigation.

609

610 Is Rictor/mTORC2 a master regulator of lipid metabolism? Recent studies of liver
611 collectively report that deleting hepatic *Rictor* results in a complex phenotype including
612 increased gluconeogenesis, decreased glycolysis, and impaired lipogenesis (Hagiwara et al.,
613 2012; Lamming et al., 2012; Yuan et al., 2012). Two studies find that hepatic *Rictor* loss
614 also decreases SREBP1c activity; however, one study suggests AKT2 mediates this function

615 ([Hagiwara et al., 2012](#)) while the other proposes an AKT-independent pathway ([Yuan et al.,](#)
616 [2012](#)). These two studies are also inconsistent with respect to how *Rictor* loss affects AKT
617 signaling and thus the role of hepatic Rictor/mTORC2 is currently controversial.
618 Nevertheless, the glucose uptake and glycolysis defect is reportedly independent of the
619 lipogenesis defect because restoring glucose flux in *Rictor*-KO hepatocytes did not rescue
620 lipogenesis ([Hagiwara et al., 2012](#)). This study also reports that fatty acid oxidation genes
621 are elevated in Rictor-deficient hepatocytes ([Hagiwara et al., 2012](#)). Thus, Rictor/mTORC2
622 may have a broad role in establishing a pro-lipogenic metabolic state. Going forward it is
623 important to determine if Rictor/mTORC2 regulates de novo lipogenesis and beta-
624 oxidation by a common or coordinate set of mechanisms, or whether one metabolic
625 deficiency is indirectly driving the other. Notably, we detect a decrease in lipogenesis gene
626 expression in P1 BAT lacking Rictor, but the increase in fatty acid oxidation gene
627 expression we first detect in 6-week mutant BAT. Thus, mitochondrial activity may
628 progressively increase in the Rictor-deficient BAT and be secondary to a lipogenesis defect.
629 Regardless, our findings support the idea that targeting lipogenesis and/or beta-oxidation
630 pathways could be one approach to treating obesity and diabetes.

631
632 Obesity develops when energy intake exceeds expenditure and one prediction is
633 that increasing BAT energy expenditure could have anti-obesity therapeutic potential
634 ([Tseng et al., 2010](#)). To achieve this goal, a much deeper understanding of how BAT utilizes
635 fuel is required ([Townsend and Tseng, 2014](#)). An important finding in our study is that
636 *Rictor*<sup>Myf5^{CKO} mice living at thermoneutrality, when challenged with an obesogenic diet,
637 induce higher levels of UCP1 and are more resistant to developing obesity and metabolic
638 disease compared to HFD-fed controls. This suggests that inhibiting mTORC2 in BAT
639 augments diet-induced thermogenesis ([Cannon and Nedergaard, 2010](#); [Feldmann et al.,](#)
640 [2009](#)); however, we cannot yet rule out that Rictor loss in other *Myf5*-lineage tissues might
641 contribute to this phenotype. It is currently being debated as to whether humans have
642 classic brown adipocytes or a potential third class of adipocyte called a brite/beige
643 adipocyte ([Nedergaard and Cannon, 2013](#)). Recent work indicates that in the neck, deep fat
644 is similar to rodent BAT and expresses high levels of UCP1 while more superficial fat
645 expresses lower UCP1 levels and has more brite/beige characteristics ([Cypess et al., 2013](#)).</sup>

646 Notably, humans typically adjust temperature to be at or around thermoneutrality (Cannon
647 and Nedergaard, 2010), and interestingly the BAT of mice living at thermoneutrality is
648 “humanized”; that is appearing more “white-fat like”, or perhaps more “brite/beige-fat” like
649 [Figure 7]. Thus, it seems likely that humans possess classic brown fat and that studies of
650 brown fat in mice will provide important insights into human BAT regulation. Continued
651 elucidation of mTORC2 pathways in BAT bioenergetics could therefore lead to novel
652 human anti-obesity therapies that target cellular energy expenditure.

653

654

655 **EXPERIMENTAL PROCEDURES**

656

657 **Antibodies and reagents**

658 Rictor (Cat# 2140), mTOR (2983), pan-AKT (9272), GSK3 β (9315), ACC (3676), ACLY
659 (4332), NDRG1 (9408) and β -actin (4970), Insulin receptor β (3025) and anti-HA-tag
660 (2367) antibodies were purchased from Cell Signaling Technologies. SREBP1 (sc-366), p70
661 S6K (sc-9027), UCP1 antibody (sc-6528), and HRP-conjugated secondary antibodies were
662 from Santa Cruz biotechnology. All phosphorylation-specific antibodies: S473-AKT (4058),
663 T308-AKT (4056), T24-FoxO1 (9464), S9-GSK3 β (9323), T1462-TSC2 (3617) and T389-
664 S6K (9234) were from Cell Signaling Technologies. 4-hydroxy-tamoxifen (4-OHT) was
665 from Toronto Research Chemicals. Indomethacin, dexamethasone, 3-isobutyl-1-
666 methylxanthine (IBMX) and all other reagents were from Sigma-Aldrich.

667

668 **Plasmids**

669 Full length AKT1 cDNA obtained by PCR amplification from pcDNA3-myr-HA-AKT1
670 (addgene #9008) was subcloned into the pCMV-HA vector. Full length AKT2 cDNA
671 obtained by PCR amplification from pBabe-myr-HA-AKT2 (addgene #9018) was subcloned
672 into the pCMV-HA vector. SGK1 cDNA (Thermo Scientific #MHS6278-202755905) was PCR
673 amplified to obtain a truncated SGK sequence (SGK-delta-60N, N-terminal 1-60 amino acids
674 deletion). Phosphomimetic constructs with indicated mutation were done by QuikChange
675 Site-Directed Mutagenesis kit (Stratagene) with appropriate primers. All cDNA constructs
676 were also transferred into pBabe-puro retroviral vector for stable expression.

677

678 **Mice**

679 *Rictor* floxed (*Rictor^{fl/fl}*) mice (Shiota et al., 2006) or *Raptor^{fl/fl}* mice (Peterson et al., 2011)
680 were crossed with *Myf5-cre* (JAX #007893)(Tallquist et al., 2000), *Ubc-CreERT2* (JAX
681 #007001)(Ruzankina et al., 2007) and *Pax7-CreERT2* (JAX #012476)(Lepper et al., 2009),
682 to make conditional or inducible knockout mice. *Rosa26-mTmG* (JAX #007676) and
683 *Rosa26-LSL-LacZ* (JAX #003474) were also obtained from Jackson laboratory. Male
684 129/C57B6 mice were used for all studies.

685

686 **Satellite cells isolation and differentiation**

687 Adult muscle satellite cells were isolated according to [\(Sherwood et al., 2004\)](#). See also
688 Supplemental Experimental Procedures.

689

690 **Gene Expression and qRT-PCR array**

691 Total RNA was isolated from cells or tissues using Qiazol (Invitrogen) and an RNeasy kit
692 (Invitrogen). Equal amounts of RNA from each individual sample were retro-transcribed to
693 cDNA using a High capacity cDNA reverse transcription kit (Applied Biosystems). *Tbp*
694 expression was used as a normalization gene in most RT-PCR experiments. A different set
695 of iBAT samples was used in RT-PCR arrays (Qiagen) according to manufacturer's
696 instruction. See also Supplemental Experimental Procedures.

697

698 **Brown preadipocytes and in vitro differentiation**

699 Primary brown adipocyte precursors (bAPC) cells were isolated from P1 neonates and
700 immortalized with pBabe-SV40 Large T antigen. To induce *Rictor* deletion *ubc-*
701 *creERT2;Rictor^{fl/fl}* cells were treated on three consecutive days with 1 μ M 4-OHT. bAPCs
702 were seeded at 4x10⁴ cells/ml and allowed reach confluence over 3 days in media
703 containing 20nM insulin, 1nM T3 (differentiation medium). On day 4, cells were induced
704 with 20nM insulin, 1nM T3, 0.125mM indomethacin, 2 μ g/mL dexamethasone and 0.5mM
705 3-isobutyl-1-methylxanthine (IBMX). Two days later the induction medium was replaced
706 with fresh differentiation medium and changed every two days until day 10. See also
707 Supplemental Experimental Procedures.

708

709 ***Ex vivo* oxygen consumption**

710 Brown adipose tissue oxygen consumption rate was measured with a Seahorse Analyzer
711 according to a previous published protocol [\(Vernochet et al., 2012\)](#). See also Supplemental
712 Experimental Procedures.

713

714 **Metabolic studies**

715 For thermoneutrality studies, 6 week-old male mice were transferred to the mouse room
716 with elevated housing temperature (30°C). Mice were kept one week in thermoneutrality

717 before using in any experiment. At 7 weeks of age, mice were started to receiving chow diet
718 (Prolab Isopro RMH3000, LabDiet) or high fat diet (45% calories from fat; ResearchDiet #
719 D12451). Mouse body weight and food intake were accessed weekly for 12 weeks. Glucose
720 tolerance tests were performed at the 11th week of the diet experiment. Overnight fasted
721 animals were subjected to GTT by i.p. injecting glucose at 2g/Kg of body weight and blood
722 glucose levels were measured by a commercially available glucose meter. A small group
723 (n=4) of mice were kept for 20 weeks of HFD for morphological studies.

724

725 **Statistics**

726 Unless otherwise stated, the results are described as mean \pm SEM. Two-way ANOVA was
727 performed where indicated. For most experiments Student's t-test was used to determine
728 statistical significance: *indicates $P < 0.05$; **, $P < 0.01$; ***, $P < 0.001$.

729

730 See also Supplemental Experimental Procedures

731

732 **AUTHOR CONTRIBUTIONS**

733

734 C-M.H. and D.A.G. conceived the project, designed the experiments, and wrote and edited
735 the manuscript. C-M.H. performed most of the experiments and D.A.G. assisted in the
736 analysis and interpretation. C.M.C. assisted with the PPAR γ rescue experiments. J.S-G.
737 assisted with the lineage tracing experiments. H.L. helped with animal experiments. C.B.C.
738 performed metabolite profiling and analysis. S.H. and A.J.W. assisted with the satellite cell
739 isolation and muscle regeneration experiments.

740

741 **ACKNOWLEDGEMENTS**

742

743 This work was supported by grants from the National Institutes of Health (R00CA129613 &
744 R01DK094004), the American Diabetes Association (ADA113BS-066), and awards from the
745 Pew Charitable Trusts and Charles Hood Foundation to D.A.G. We thank Yuefeng Tang,
746 Xiaohao Yao, and Christine Powers for technical assistance, Morris Birnbaum for providing
747 *Akt1&2* floxed mice, and Marcus Cooper for the PPAR γ 2 construct. Metabolic cage studies
748 were performed in the UMass Mouse Phenotype Center (DK09300). The authors declare
749 no conflict of interests.

750

751

752

753

754

755

756 **REFERENCES**

- 757
- 758 Balcke, G.U., Kolle, S.N., Kamp, H., Bethan, B., Looser, R., Wagner, S., Landsiedel, R., and van
759 Ravenzwaay, B. (2011). Linking energy metabolism to dysfunctions in mitochondrial
760 respiration--a metabolomics in vitro approach. *Toxicology letters* 203, 200-209.
- 761 Banks, A.S., Kim-Muller, J.Y., Mastracci, T.L., Kofler, N.M., Qiang, L., Haeusler, R.A., Jurczak,
762 M.J., Laznik, D., Heinrich, G., Samuel, V.T., Shulman, G.I., Papaioannou, V.E., and Accili, D.
763 (2011). Dissociation of the glucose and lipid regulatory functions of FoxO1 by targeted
764 knockin of acetylation-defective alleles in mice. *Cell metabolism* 14, 587-597.
- 765 Ben-Sahra, I., Howell, J.J., Asara, J.M., and Manning, B.D. (2013). Stimulation of de Novo
766 Pyrimidine Synthesis by Growth Signaling Through mTOR and S6K1. *Science*.
- 767 Bentzinger, C.F., Romanino, K., Cloetta, D., Lin, S., Mascarenhas, J.B., Oliveri, F., Xia, J.,
768 Casanova, E., Costa, C.F., Brink, M., Zorzato, F., Hall, M.N., and Ruegg, M.A. (2008). Skeletal
769 muscle-specific ablation of raptor, but not of rictor, causes metabolic changes and results in
770 muscle dystrophy. *Cell metabolism* 8, 411-424.
- 771 Cannon, B., and Nedergaard, J. (2004). Brown adipose tissue: function and physiological
772 significance. *Physiological reviews* 84, 277-359.
- 773 Cannon, B., and Nedergaard, J. (2010). Metabolic consequences of the presence or absence
774 of the thermogenic capacity of brown adipose tissue in mice (and probably in humans). *Int*
775 *J Obes (Lond)* 34 Suppl 1, S7-16.
- 776 Cederberg, A., Gronning, L.M., Ahren, B., Tasken, K., Carlsson, P., and Enerback, S. (2001).
777 FOXC2 is a winged helix gene that counteracts obesity, hypertriglyceridemia, and diet-
778 induced insulin resistance. *Cell* 106, 563-573.
- 779 Cho, H., Mu, J., Kim, J.K., Thorvaldsen, J.L., Chu, Q., Crenshaw, E.B., 3rd, Kaestner, K.H.,
780 Bartolomei, M.S., Shulman, G.I., and Birnbaum, M.J. (2001). Insulin resistance and a diabetes
781 mellitus-like syndrome in mice lacking the protein kinase Akt2 (PKB beta). *Science* 292,
782 1728-1731.
- 783 Cristancho, A.G., and Lazar, M.A. (2011). Forming functional fat: a growing understanding of
784 adipocyte differentiation. *Nature reviews. Molecular cell biology* 12, 722-734.
- 785 Cybulski, N., Polak, P., Auwerx, J., Ruegg, M.A., and Hall, M.N. (2009). mTOR complex 2 in
786 adipose tissue negatively controls whole-body growth. *Proceedings of the National*
787 *Academy of Sciences of the United States of America* 106, 9902-9907.
- 788 Cypess, A.M., Lehman, S., Williams, G., Tal, I., Rodman, D., Goldfine, A.B., Kuo, F.C., Palmer,
789 E.L., Tseng, Y.H., Doria, A., Kolodny, G.M., and Kahn, C.R. (2009). Identification and
790 importance of brown adipose tissue in adult humans. *The New England journal of medicine*
791 360, 1509-1517.

792 Cypess, A.M., White, A.P., Vernochet, C., Schulz, T.J., Xue, R., Sass, C.A., Huang, T.L., Roberts-
793 Toler, C., Weiner, L.S., Sze, C., Chacko, A.T., Deschamps, L.N., Herder, L.M., Truchan, N.,
794 Glasgow, A.L., Holman, A.R., Gavrila, A., Hasselgren, P.O., Mori, M.A., Molla, M., and Tseng,
795 Y.H. (2013). Anatomical localization, gene expression profiling and functional
796 characterization of adult human neck brown fat. *Nature medicine* 19, 635-639.

797 Czech, M.P., Tencerova, M., Pedersen, D.J., and Aouadi, M. (2013). Insulin signalling
798 mechanisms for triacylglycerol storage. *Diabetologia*.

799 Eijkelenboom, A., and Burgering, B.M. (2013). FOXOs: signalling integrators for
800 homeostasis maintenance. *Nature reviews. Molecular cell biology* 14, 83-97.

801 Fasshauer, M., Klein, J., Kriauciunas, K.M., Ueki, K., Benito, M., and Kahn, C.R. (2001).
802 Essential role of insulin receptor substrate 1 in differentiation of brown adipocytes.
803 *Molecular and cellular biology* 21, 319-329.

804 Feldmann, H.M., Golozoubova, V., Cannon, B., and Nedergaard, J. (2009). UCP1 ablation
805 induces obesity and abolishes diet-induced thermogenesis in mice exempt from thermal
806 stress by living at thermoneutrality. *Cell metabolism* 9, 203-209.

807 Filhoulaud, G., Guilmeau, S., Dentin, R., Girard, J., and Postic, C. (2013). Novel insights into
808 ChREBP regulation and function. *Trends in endocrinology and metabolism: TEM* 24, 257-
809 268.

810 Garcia-Martinez, J.M., and Alessi, D.R. (2008). mTOR complex 2 (mTORC2) controls
811 hydrophobic motif phosphorylation and activation of serum- and glucocorticoid-induced
812 protein kinase 1 (SGK1). *The Biochemical journal* 416, 375-385.

813 Garofalo, R.S., Orena, S.J., Rafidi, K., Torchia, A.J., Stock, J.L., Hildebrandt, A.L., Coskran, T.,
814 Black, S.C., Brees, D.J., Wicks, J.R., McNeish, J.D., and Coleman, K.G. (2003). Severe diabetes,
815 age-dependent loss of adipose tissue, and mild growth deficiency in mice lacking Akt2/PKB
816 beta. *J Clin Invest* 112, 197-208.

817 Gerin, I., Bommer, G.T., Lidell, M.E., Cederberg, A., Enerback, S., and Macdougald, O.A.
818 (2009). On the role of FOX transcription factors in adipocyte differentiation and insulin-
819 stimulated glucose uptake. *The Journal of biological chemistry* 284, 10755-10763.

820 Gesta, S., Tseng, Y.H., and Kahn, C.R. (2007). Developmental origin of fat: tracking obesity to
821 its source. *Cell* 131, 242-256.

822 Guertin, D.A., Stevens, D.M., Saitoh, M., Kinkel, S., Crosby, K., Sheen, J.H., Mullholland, D.J.,
823 Magnuson, M.A., Wu, H., and Sabatini, D.M. (2009). mTOR complex 2 is required for the
824 development of prostate cancer induced by Pten loss in mice. *Cancer cell* 15, 148-159.

825 Guertin, D.A., Stevens, D.M., Thoreen, C.C., Burds, A.A., Kalaany, N.Y., Moffat, J., Brown, M.,
826 Fitzgerald, K.J., and Sabatini, D.M. (2006). Ablation in mice of the mTORC components

827 raptor, rictor, or mLST8 reveals that mTORC2 is required for signaling to Akt-FOXO and
828 PKCalpha, but not S6K1. *Developmental cell* 11, 859-871.

829 Hagiwara, A., Cornu, M., Cybulski, N., Polak, P., Betz, C., Trapani, F., Terracciano, L., Heim,
830 M.H., Ruegg, M.A., and Hall, M.N. (2012). Hepatic mTORC2 Activates Glycolysis and
831 Lipogenesis through Akt, Glucokinase, and SREBP1c. *Cell metabolism* 15, 725-738.

832 Harms, M., and Seale, P. (2013). Brown and beige fat: development, function and
833 therapeutic potential. *Nature medicine* 19, 1252-1263.

834 Harms, M.J., Ishibashi, J., Wang, W., Lim, H.W., Goyama, S., Sato, T., Kurokawa, M., Won, K.J.,
835 and Seale, P. (2014). Prdm16 is required for the maintenance of brown adipocyte identity
836 and function in adult mice. *Cell metabolism* 19, 593-604.

837 Infantino, V., Iacobazzi, V., De Santis, F., Mastrapasqua, M., and Palmieri, F. (2007).
838 Transcription of the mitochondrial citrate carrier gene: role of SREBP-1, upregulation by
839 insulin and downregulation by PUFA. *Biochemical and biophysical research*
840 *communications* 356, 249-254.

841 Jacinto, E., Facchinetti, V., Liu, D., Soto, N., Wei, S., Jung, S.Y., Huang, Q., Qin, J., and Su, B.
842 (2006). SIN1/MIP1 maintains rictor-mTOR complex integrity and regulates Akt
843 phosphorylation and substrate specificity. *Cell* 127, 125-137.

844 Kajimura, S., Seale, P., and Spiegelman, B.M. (2010). Transcriptional control of brown fat
845 development. *Cell metabolism* 11, 257-262.

846 Kumar, A., Harris, T.E., Keller, S.R., Choi, K.M., Magnuson, M.A., and Lawrence, J.C., Jr. (2008).
847 Muscle-specific deletion of rictor impairs insulin-stimulated glucose transport and
848 enhances Basal glycogen synthase activity. *Molecular and cellular biology* 28, 61-70.

849 Kumar, A., Lawrence, J.C., Jr., Jung, D.Y., Ko, H.J., Keller, S.R., Kim, J.K., Magnuson, M.A., and
850 Harris, T.E. (2010). Fat cell-specific ablation of rictor in mice impairs insulin-regulated fat
851 cell and whole-body glucose and lipid metabolism. *Diabetes* 59, 1397-1406.

852 Lamming, D.W., Ye, L., Katajisto, P., Goncalves, M.D., Saitoh, M., Stevens, D.M., Davis, J.G.,
853 Salmon, A.B., Richardson, A., Ahima, R.S., Guertin, D.A., Sabatini, D.M., and Baur, J.A. (2012).
854 Rapamycin-induced insulin resistance is mediated by mTORC2 loss and uncoupled from
855 longevity. *Science* 335, 1638-1643.

856 Laplante, M., and Sabatini, D.M. (2012). mTOR Signaling in Growth Control and Disease. *Cell*
857 149, 274-293.

858 Lee, K.Y., Russell, S.J., Ussar, S., Boucher, J., Vernochet, C., Mori, M.A., Smyth, G., Rourk, M.,
859 Cederquist, C., Rosen, E.D., Kahn, B.B., and Kahn, C.R. (2013). Lessons on conditional gene
860 targeting in mouse adipose tissue. *Diabetes* 62, 864-874.

861 Lepper, C., Conway, S.J., and Fan, C.M. (2009). Adult satellite cells and embryonic muscle
862 progenitors have distinct genetic requirements. *Nature* 460, 627-631.

863 Martinez-Lopez, N., Athonvarangkul, D., Sahu, S., Coletto, L., Zong, H., Bastie, C.C., Pessin, J.E.,
864 Schwartz, G.J., and Singh, R. (2013). Autophagy in Myf5+ progenitors regulates energy and
865 glucose homeostasis through control of brown fat and skeletal muscle development. *EMBO*
866 *reports* 14, 795-803.

867 Masui, K., Tanaka, K., Akhavan, D., Babic, I., Gini, B., Matsutani, T., Iwanami, A., Liu, F., Villa,
868 G.R., Gu, Y., Campos, C., Zhu, S., Yang, H., Yong, W.H., Cloughesy, T.F., Mellinghoff, I.K.,
869 Cavenee, W.K., Shaw, R.J., and Mischel, P.S. (2013). mTOR Complex 2 Controls Glycolytic
870 Metabolism in Glioblastoma through FoxO Acetylation and Upregulation of c-Myc. *Cell*
871 *metabolism*.

872 Mizuarai, S., Miki, S., Araki, H., Takahashi, K., and Kotani, H. (2005). Identification of
873 dicarboxylate carrier Slc25a10 as malate transporter in de novo fatty acid synthesis. *The*
874 *Journal of biological chemistry* 280, 32434-32441.

875 Mullican, S.E., Tomaru, T., Gaddis, C.A., Peed, L.C., Sundaram, A., and Lazar, M.A. (2013). A
876 novel adipose-specific gene deletion model demonstrates potential pitfalls of existing
877 methods. *Mol Endocrinol* 27, 127-134.

878 Muzumdar, M.D., Tasic, B., Miyamichi, K., Li, L., and Luo, L. (2007). A global double-
879 fluorescent Cre reporter mouse. *Genesis* 45, 593-605.

880 Nedergaard, J., Bengtsson, T., and Cannon, B. (2007). Unexpected evidence for active brown
881 adipose tissue in adult humans. *Am J Physiol Endocrinol Metab* 293, E444-452.

882 Nedergaard, J., and Cannon, B. (2010). The changed metabolic world with human brown
883 adipose tissue: therapeutic visions. *Cell metabolism* 11, 268-272.

884 Nedergaard, J., and Cannon, B. (2013). How brown is brown fat? It depends where you look.
885 *Nature medicine* 19, 540-541.

886 Ohno, H., Shinoda, K., Ohyama, K., Sharp, L.Z., and Kajimura, S. (2013). EHMT1 controls
887 brown adipose cell fate and thermogenesis through the PRDM16 complex. *Nature* 504,
888 163-167.

889 Ortega-Molina, A., Efeyan, A., Lopez-Guadamillas, E., Munoz-Martin, M., Gomez-Lopez, G.,
890 Canamero, M., Mulero, F., Pastor, J., Martinez, S., Romanos, E., Mar Gonzalez-Barroso, M.,
891 Rial, E., Valverde, A.M., Bischoff, J.R., and Serrano, M. (2012). Pten positively regulates
892 brown adipose function, energy expenditure, and longevity. *Cell metabolism* 15, 382-394.

893 Pearce, L.R., Komander, D., and Alessi, D.R. (2010). The nuts and bolts of AGC protein
894 kinases. *Nature reviews. Molecular cell biology* 11, 9-22.

895 Peterson, T.R., Sengupta, S.S., Harris, T.E., Carmack, A.E., Kang, S.A., Balderas, E., Guertin,
896 D.A., Madden, K.L., Carpenter, A.E., Finck, B.N., and Sabatini, D.M. (2011). mTOR complex 1
897 regulates lipin 1 localization to control the SREBP pathway. *Cell* 146, 408-420.

898 Robitaille, A.M., Christen, S., Shimobayashi, M., Cornu, M., Fava, L.L., Moes, S., Prescianotto-
899 Baschong, C., Sauer, U., Jenoe, P., and Hall, M.N. (2013). Quantitative Phosphoproteomics
900 Reveal mTORC1 Activates de Novo Pyrimidine Synthesis. *Science*.

901 Ruzankina, Y., Pinzon-Guzman, C., Asare, A., Ong, T., Pontano, L., Cotsarelis, G., Zediak, V.P.,
902 Velez, M., Bhandoola, A., and Brown, E.J. (2007). Deletion of the developmentally essential
903 gene ATR in adult mice leads to age-related phenotypes and stem cell loss. *Cell stem cell* 1,
904 113-126.

905 Sanchez-Gurmaches, J., and Guertin, D.A. (2014a). Adipocyte lineages: tracing back the
906 origins of fat. *Biochimica et biophysica acta* 1842, 340-351.

907 Sanchez-Gurmaches, J., and Guertin, D.A. (2014b). Adipocytes arise from multiple lineages
908 that are heterogeneously and dynamically distributed. *Nature communications* in press.

909 Sanchez-Gurmaches, J., Hung, C.M., Sparks, C.A., Tang, Y., Li, H., and Guertin, D.A. (2012).
910 PTEN loss in the Myf5 lineage redistributes body fat and reveals subsets of white
911 adipocytes that arise from Myf5 precursors. *Cell metabolism* 16, 348-362.

912 Sarbassov, D.D., Guertin, D.A., Ali, S.M., and Sabatini, D.M. (2005). Phosphorylation and
913 regulation of Akt/PKB by the rictor-mTOR complex. *Science* 307, 1098-1101.

914 Schulz, T.J., Huang, P., Huang, T.L., Xue, R., McDougall, L.E., Townsend, K.L., Cypess, A.M.,
915 Mishina, Y., Gussoni, E., and Tseng, Y.H. (2013). Brown-fat paucity due to impaired BMP
916 signalling induces compensatory browning of white fat. *Nature* 495, 379-383.

917 Schulz, T.J., and Tseng, Y.H. (2013). Brown adipose tissue: development, metabolism and
918 beyond. *The Biochemical journal* 453, 167-178.

919 Seale, P., Bjork, B., Yang, W., Kajimura, S., Chin, S., Kuang, S., Scime, A., Devarakonda, S.,
920 Conroe, H.M., Erdjument-Bromage, H., Tempst, P., Rudnicki, M.A., Beier, D.R., and
921 Spiegelman, B.M. (2008). PRDM16 controls a brown fat/skeletal muscle switch. *Nature* 454,
922 961-967.

923 Sherwood, R.I., Christensen, J.L., Conboy, I.M., Conboy, M.J., Rando, T.A., Weissman, I.L., and
924 Wagers, A.J. (2004). Isolation of adult mouse myogenic progenitors: functional
925 heterogeneity of cells within and engrafting skeletal muscle. *Cell* 119, 543-554.

926 Shiota, C., Woo, J.T., Lindner, J., Shelton, K.D., and Magnuson, M.A. (2006). Multiallelic
927 disruption of the rictor gene in mice reveals that mTOR complex 2 is essential for fetal
928 growth and viability. *Developmental cell* 11, 583-589.

- 929 Tallquist, M.D., Weismann, K.E., Hellstrom, M., and Soriano, P. (2000). Early myotome
930 specification regulates PDGFA expression and axial skeleton development. *Development*
931 127, 5059-5070.
- 932 Townsend, K.L., and Tseng, Y.H. (2014). Brown fat fuel utilization and thermogenesis.
933 *Trends in endocrinology and metabolism: TEM* 25, 168-177.
- 934 Tseng, Y.H., Butte, A.J., Kokkotou, E., Yechoor, V.K., Taniguchi, C.M., Kriauciunas, K.M.,
935 Cypess, A.M., Niinobe, M., Yoshikawa, K., Patti, M.E., and Kahn, C.R. (2005). Prediction of
936 preadipocyte differentiation by gene expression reveals role of insulin receptor substrates
937 and necdin. *Nature cell biology* 7, 601-611.
- 938 Tseng, Y.H., Cypess, A.M., and Kahn, C.R. (2010). Cellular bioenergetics as a target for
939 obesity therapy. *Nature reviews. Drug discovery* 9, 465-482.
- 940 Tseng, Y.H., Kokkotou, E., Schulz, T.J., Huang, T.L., Winnay, J.N., Taniguchi, C.M., Tran, T.T.,
941 Suzuki, R., Espinoza, D.O., Yamamoto, Y., Ahrens, M.J., Dudley, A.T., Norris, A.W., Kulkarni,
942 R.N., and Kahn, C.R. (2008). New role of bone morphogenetic protein 7 in brown
943 adipogenesis and energy expenditure. *Nature* 454, 1000-1004.
- 944 van Marken Lichtenbelt, W.D., Vanhomerig, J.W., Smulders, N.M., Drossaerts, J.M.,
945 Kemerink, G.J., Bouvy, N.D., Schrauwen, P., and Teule, G.J. (2009). Cold-activated brown
946 adipose tissue in healthy men. *The New England journal of medicine* 360, 1500-1508.
- 947 Vernochet, C., Mourier, A., Bezy, O., Macotela, Y., Boucher, J., Rardin, M.J., An, D., Lee, K.Y.,
948 Ilkayeva, O.R., Zingaretti, C.M., Emanuelli, B., Smyth, G., Cinti, S., Newgard, C.B., Gibson, B.W.,
949 Larsson, N.G., and Kahn, C.R. (2012). Adipose-specific deletion of TFAM increases
950 mitochondrial oxidation and protects mice against obesity and insulin resistance. *Cell*
951 *metabolism* 16, 765-776.
- 952 Virtanen, K.A., Lidell, M.E., Orava, J., Heglind, M., Westergren, R., Niemi, T., Taittonen, M.,
953 Laine, J., Savisto, N.J., Enerback, S., and Nuutila, P. (2009). Functional brown adipose tissue
954 in healthy adults. *The New England journal of medicine* 360, 1518-1525.
- 955 Walden, T.B., Hansen, I.R., Timmons, J.A., Cannon, B., and Nedergaard, J. (2011). Recruited
956 versus nonrecruited molecular signatures of brown, "brite" and white adipose tissues. *Am J*
957 *Physiol Endocrinol Metab*.
- 958 Wang, F., Mullican, S.E., DiSpirito, J.R., Peed, L.C., and Lazar, M.A. (2013). Lipoatrophy and
959 severe metabolic disturbance in mice with fat-specific deletion of PPARgamma.
960 *Proceedings of the National Academy of Sciences of the United States of America* 110,
961 18656-18661.
- 962 Yao, Y., Suraokar, M., Darnay, B.G., Hollier, B.G., Shaiken, T.E., Asano, T., Chen, C.H., Chang,
963 B.H., Lu, Y., Mills, G.B., Sarbassov, D., Mani, S.A., Abbruzzese, J.L., and Reddy, S.A. (2013).
964 BSTA promotes mTORC2-mediated phosphorylation of Akt1 to suppress expression of
965 FoxC2 and stimulate adipocyte differentiation. *Science signaling* 6, ra2.

966 Yuan, M., Pino, E., Wu, L., Kacergis, M., and Soukas, A.A. (2012). Identification of Akt-
967 independent regulation of hepatic lipogenesis by mammalian target of rapamycin (mTOR)
968 complex 2. *The Journal of biological chemistry* 287, 29579-29588.
969
970

971 **FIGURE LEGENDS**

972

973 **Figure 1. Post-natal brown and white adipose tissue growth requires Rictor**

974 (A) Growth curve of control and *Rictor^{Myf5cKO}* mice (n=13; bars represent mean ± SEM; t-
975 test; *p<0.05, **p<0.01, ***p<0.001).

976 (B) (Left) Mass of BATs as a percent of total body weight (6-wks) (n=19-21; bars represent
977 mean ± SEM; t-test; ***p<0.001) and (Right) representative image of control and mutant
978 iBAT (6-wks).

979 (C) (Left) Mass of WATs expressed as a percent of total body weight (6-wks) (n=14-16;
980 bars represent mean ± SEM; t-test; **p<0.01, ***p<0.001) and (Right) representative image
981 of control and mutant rWAT (6-wks).

982 (D) Mass of lean tissues expressed as a percent of total body weight (6-wks) (n=15-19; bars
983 represent mean ± SEM; t-test; ***p<0.001).

984 (E) Western blots of lysates prepared from the indicated tissues (6-wks).

985 (F) Tissue mass expressed as average weight (mg) at 6-wks and 6-mos of age (n= 14-21 for
986 6-wks mice; n=7 for 6-mos mice; bars represent mean ± SEM; t-test; ***p<0.001).

987 See also Figure S1.

988

989 **Figure 2. Brown and white adipocytes lacking *Rictor* are smaller and multilocular**

990 (A) H&E stains of interscapular brown adipose tissue (iBAT) at embryonic day 18.5
991 (E18.5), postnatal day 1 (P1), 6 week (6 w) and 6 months (6 m).

992 (B) H&E stains of retroperitoneal (rWAT) and anterior subcutaneous (asWAT) at 6-wks.

993 (C) Representative images of mTFP and mGFP labeled rWAT and asWAT adipocytes.

994 Enlarged images are indicated by white box at 63X.

995 See also Figure S2.

996

997 **Figure 3. Rictor-deficient brown adipocytes have a lipid metabolism defect despite**
998 **having normal pan-AKT signaling**

999 (A) Western blots of the indicated total and phospho-proteins using 6-wks iBAT lysates.

1000 Mice were fasted overnight and re-fed for 45mins prior to preparing lysates.

1001 (B-D) qRT-PCR of the indicated genes in P1 (n=6) and 6wk (n=8) iBAT (bars represent
1002 mean \pm SEM; t-test; *p<0.05, **p<0.01)

1003 See also Figure S3.

1004

1005 **Figure 4. Mitochondrial activity is elevated in Rictor-deficient BAT**

1006 (A) qRT-PCR of mitochondrial genes in P1 (n=6) and 6wk iBAT (n=8) (bars represent mean
1007 \pm SEM; t-test; *p<0.05, **p<0.01)

1008 (B) Differentially expressed mitochondrial functional genes found using qRT-PCR arrays.
1009 Data is shown as fold regulation (conditional KO relative to control) and all genes listed are
1010 significantly different between 6wk *control* and *Rictor^{my5ckO}* iBAT (n=4; t-test; p<0.05)

1011 (C) Representative immunofluorescence images of mitochondrial Cox IV staining in 6wk
1012 iBAT (n=3).

1013 (D) (Left) Representative TEM images of 6wk iBAT and (Right) quantification of
1014 mitochondria size (n=3; bars represent mean \pm SEM; t-test; ***p<0.001)

1015 (E) Oxygen consumption iBAT measured *ex vivo* using a Seahorse Flux Analyzer (12 wks,
1016 n=5; values are normalized to DNA content; bars represent mean \pm SEM; t-test; *p<0.05)

1017 (F) (Left) qRT-PCR of *Ucp1* mRNA expression in iBAT with or without cold exposure (n=3
1018 for 22°C; n=4 for 4°C; bars represent mean \pm SEM; two-way ANOVA; ***P<0.001) and

1019 (Right) rectal temperature in acute cold challenged mice (n=4; bars represent mean \pm SEM;
1020 t-test; no significant difference).

1021 See also Figure S4.

1022

1023 **Figure 5. Rictor is required for brown adipocyte differentiation in vitro**

1024 (A) Western immunoblots showing phosphorylation of AKT and its effectors in control and
1025 *Rictor^{iKO}* brown preadipocytes. Cells were serum deprived for 3 hours then stimulated with
1026 0, 5, 25, 120, or 600nM insulin respectively for 15 minutes prior to lysis.

1027 (B) Oil Red O staining of control and *Rictor^{iKO}* cells after differentiation.

1028 (C) Western immunoblots of the indicated total and phospho- proteins on each of the
1029 indicated days of differentiation.

1030 (D) qRT-PCR of mRNA levels for the indicated differentiation-related genes (n=3; bars
1031 represent mean \pm SEM; t-test; *p<0.05, ***p<0.001).

1032 (E) Western immunoblots of the indicated total and phospho proteins on each of the
1033 indicated days of differentiation (samples correspond with panel (C)).
1034 (F) Western immunoblots of cell lysates collected at day 10 of differentiation. M indicates
1035 mock transfection; V indicates cells transfected with empty vector; $\gamma 2$ indicates cells
1036 transfected with recombinant PPAR $\gamma 2$. Arrows point to the $\gamma 1$ and $\gamma 2$ isoforms.
1037 (G) Oil Red O staining of differentiated cells described in (F).
1038 See also Figure S5.

1039

1040 **Figure 6. Recombinant AKT1-S473D or BMP7 supplementation rescue**
1041 **differentiation in the absence of Rictor**

1042 (A) Oil Red O staining of differentiated control cells (vehicle-treated) and *Rictor^{iKO}* cells (4-
1043 OHT treated) that stably express the indicated recombinant constructs or empty vector.
1044 (B) Western immunoblots of lysates prepared from the differentiated cells in (A).
1045 (C) Western immunoblots of lysates prepared from undifferentiated control and *Rictor^{iKO}*
1046 cells. Cells were serum deprived for 3 hours, then stimulated with FBS or BMP7 (3.2nM)
1047 for 15 minutes.
1048 (D) Oil Red O staining of differentiated control (vehicle-treated) and *Rictor^{iKO}* (4-OHT
1049 treated) cells in the presence or absence of BMP7. BMP7 (3.2nM) was added at day 1 in the
1050 differentiation protocol.
1051 (E) Western immunoblots of lysates prepared from differentiated cells in (D).
1052 See also Figure S6.

1053

1054 **Figure 7. *Rictor^{Myf5cKO}* mice exempt from thermal stress and consuming a high fat diet**
1055 **are resistant to obesity and metabolic disease**

1056 (A) Weekly weight gain of control and *Rictor^{Myf5cKO}* mice during 12-weeks of each normal
1057 chow diet (chow) or high fat diet (HFD) (n=8 for control and n=12 for KO in chow; n=10 for
1058 both genotypes on HFD; bars represent mean \pm SEM; t-test; *p<0.05) The control mice
1059 initially weighed 21.63 \pm 0.812g in the chow group and 21.24 \pm 0.621 in the HFD group; The
1060 *Rictor^{Myf5cKO}* mice initially weighted 19.42 \pm 0.305g in the chow group and 19.32 \pm 0.348 in
1061 the HFD group.

1062 (B) Total energy intake (MJ) during the feeding regimen described in (A). Control mice
1063 consumed 3.75 ± 0.557 g of chow and 2.81 ± 0.120 g of HFD; *Rictor^{Myf5^{CKO}}* mice consumed
1064 3.85 ± 0.237 g of chow and 2.95 ± 0.354 g of HFD.

1065 (C) Metabolic efficiency was determined as the amount of body weight increase (g) per MJ
1066 food consumed (n=8 for control and n=12 for KO on chow; n=10 for both genotypes on
1067 HFD; bars represent mean \pm SEM; two-way ANOVA; *p<0.05, ***p<0.001).

1068 (D) Mass (mg) of the indicated tissues collected from control and KO mice after 12 weeks
1069 on chow or HFD. (n=8 for control and n=12 for KO on chow; n=10 for both genotypes on
1070 HFD; bars represent mean \pm SEM; two-way ANOVA; *p<0.05, ***p<0.001).

1071 (E-F) H&E staining of iBAT and pgWAT and Oil red O staining of livers after 12-weeks of
1072 eating chow diet (E) or high fat diet (F).

1073 (G) qRT-PCR of the indicated brown and white fat genes in iBAT from chow or HFD mice
1074 (n=8 for control and n=12 for KO on chow; n=10 for both genotypes on HFD; bars
1075 represent mean \pm SEM; two-way ANOVA; *p<0.05, **p<0.01, ***p<0.001; # indicates
1076 significant difference over the control chow group).

1077 (H) qRT-PCR of the indicated metabolic genes in iBAT from chow or HFD mice (n=8 for
1078 control and n=12 for KO in chow; n=10 for both genotypes in HFD; bars represent mean \pm
1079 SEM; two-way ANOVA; *p<0.05, **p<0.01, ***p<0.001; # indicates significant difference
1080 over the control chow group).

1081 (I) Western immunoblot for UCP1 and the indicated control proteins using lysates
1082 prepared from iBAT.

1083 See also Figure S7.

1084

1085

1086

1087

1088

1089

1090

1091

1092

1093

1094

Figure 1

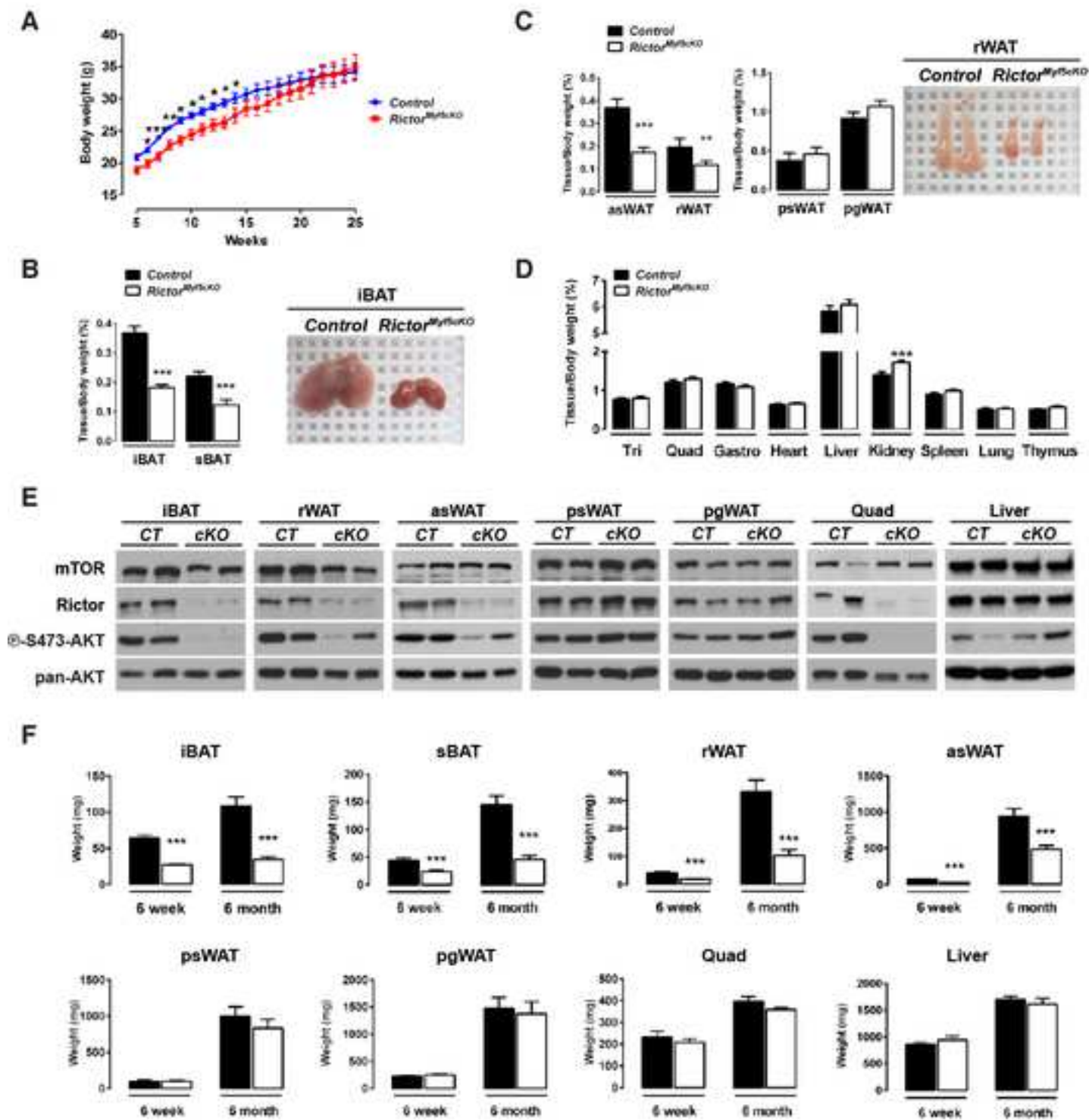
[Click here to download high resolution image](#)

Figure 2
[Click here to download high resolution image](#)

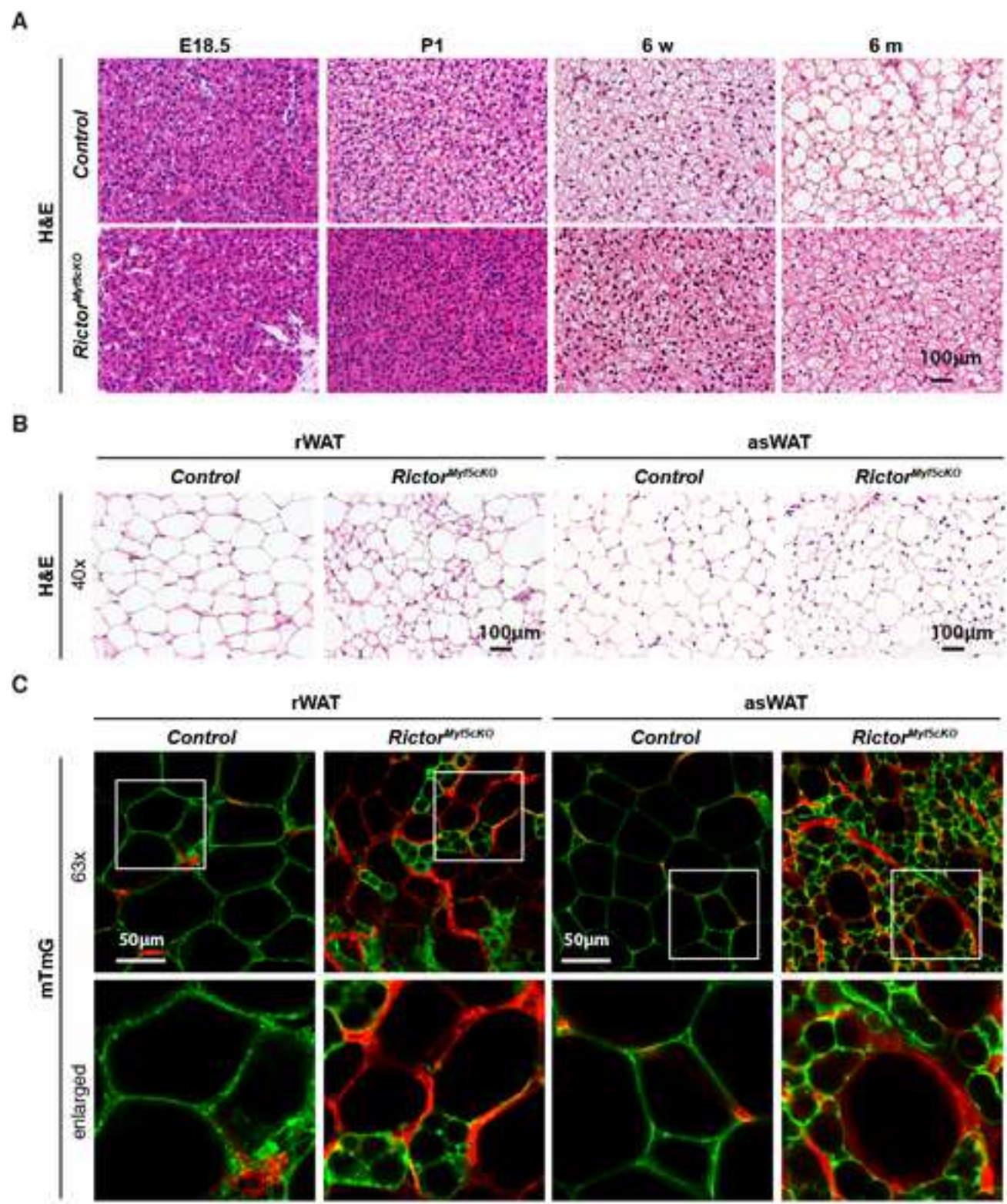


Figure 3
[Click here to download high resolution image](#)

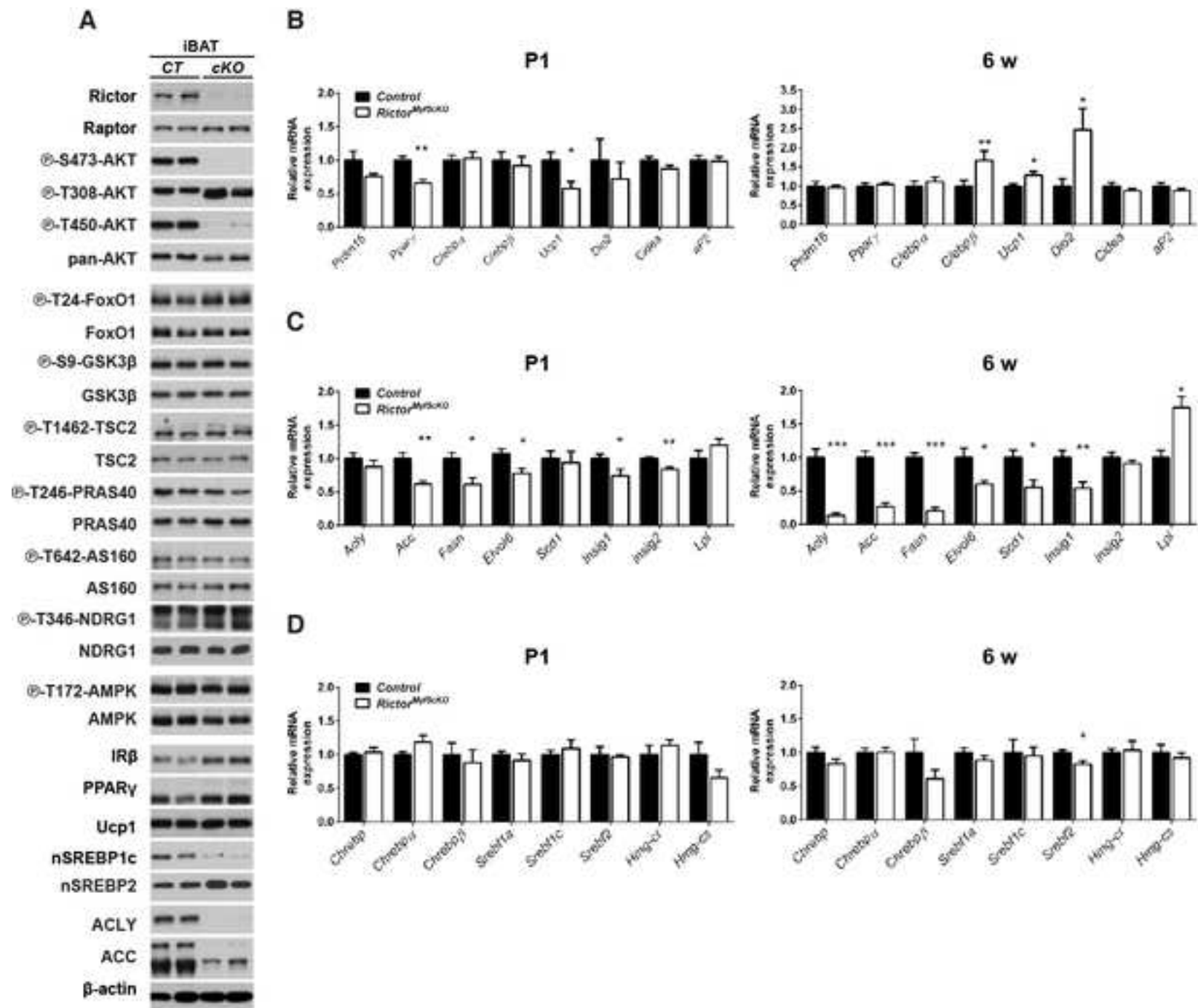


Figure 4
[Click here to download high resolution image](#)

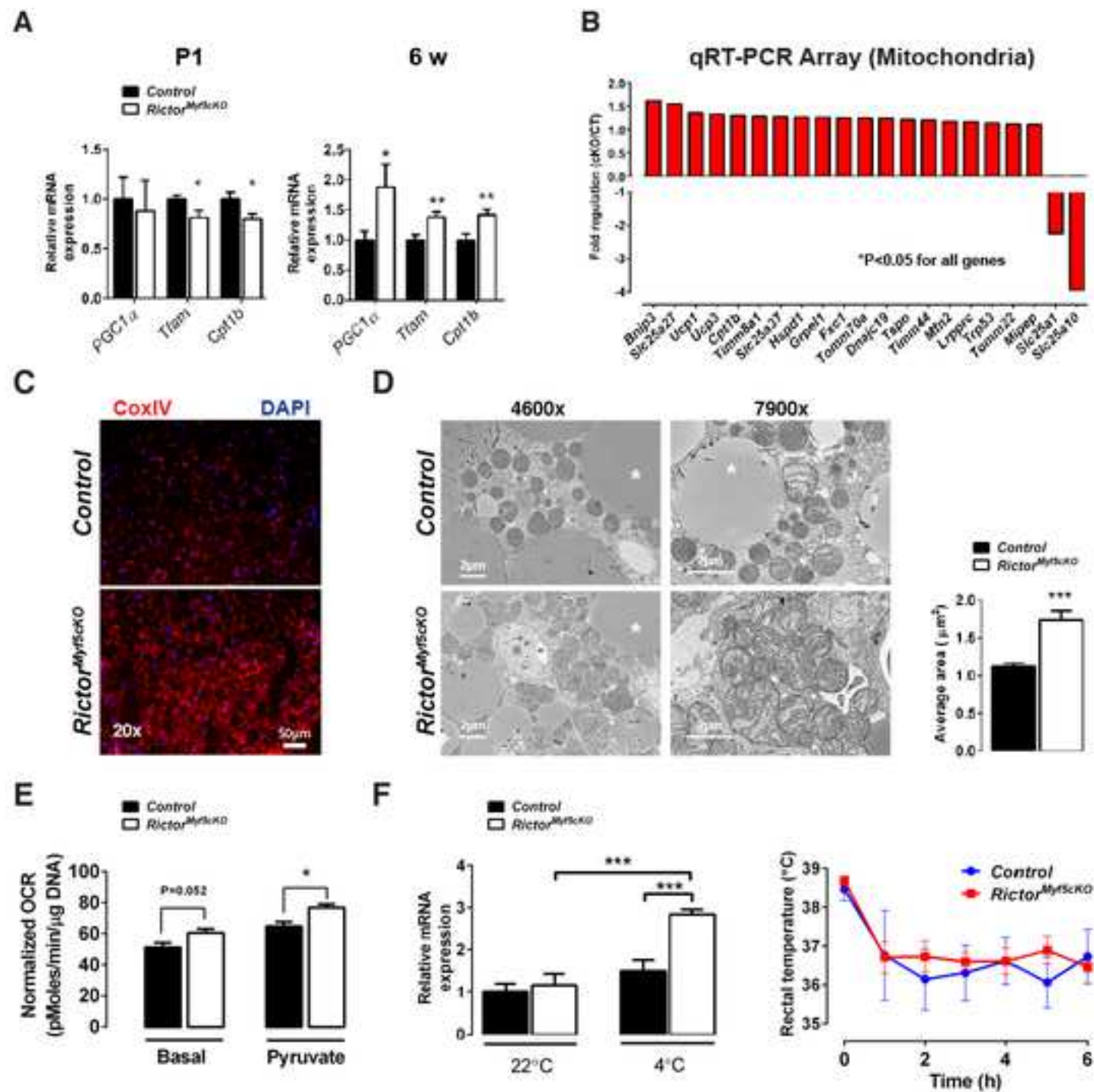


Figure 5
[Click here to download high resolution image](#)

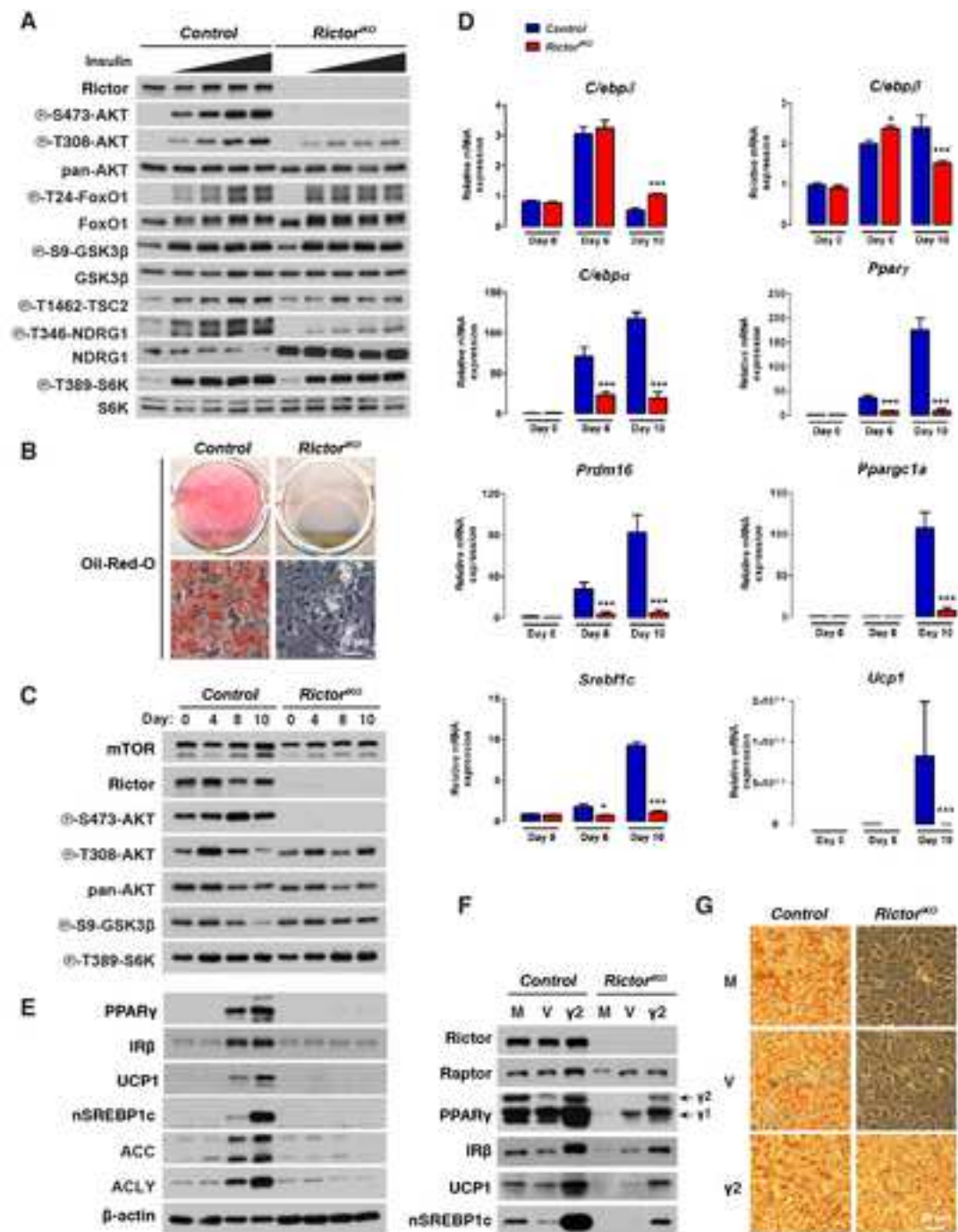


Figure 6
[Click here to download high resolution image](#)

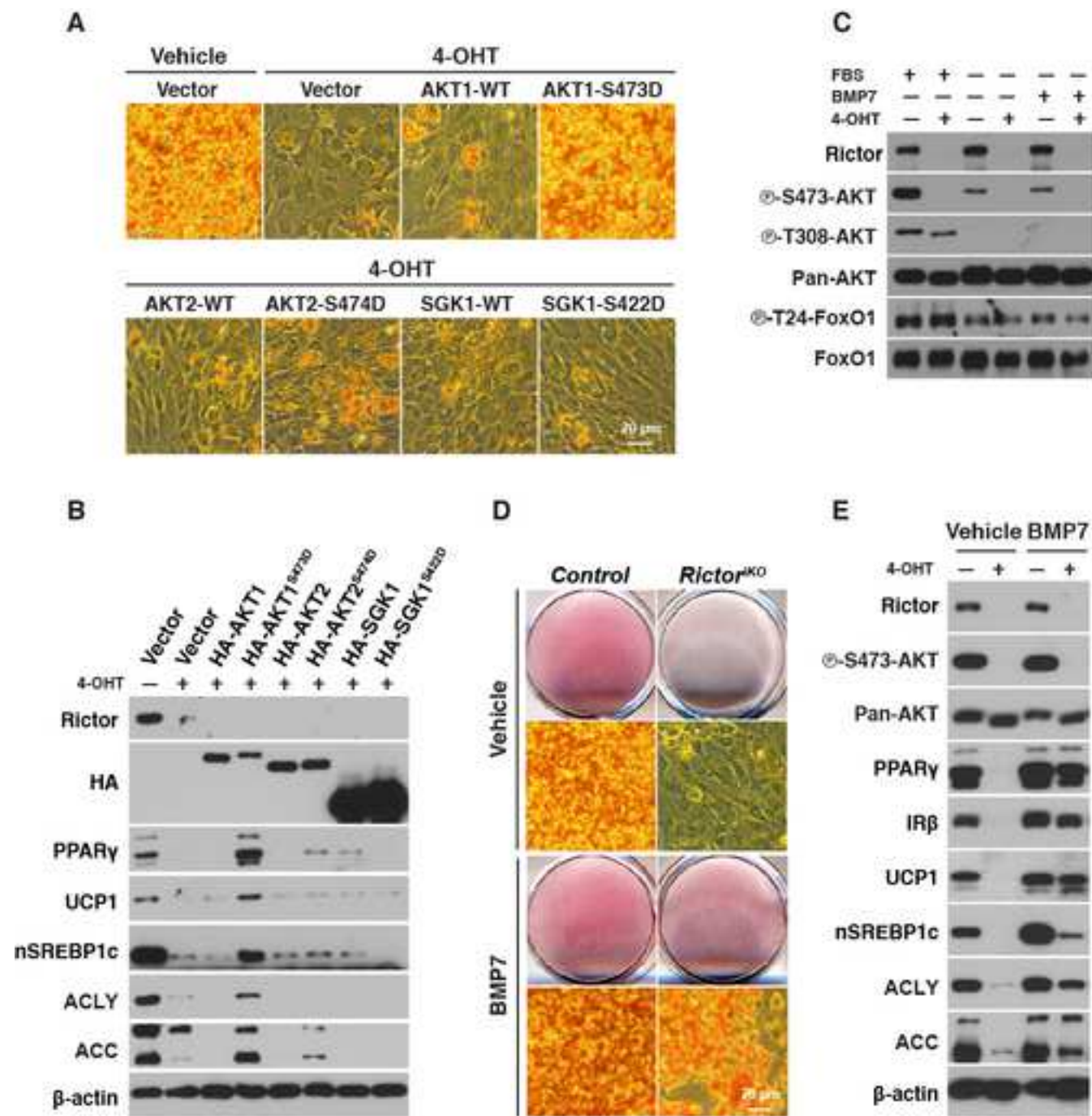
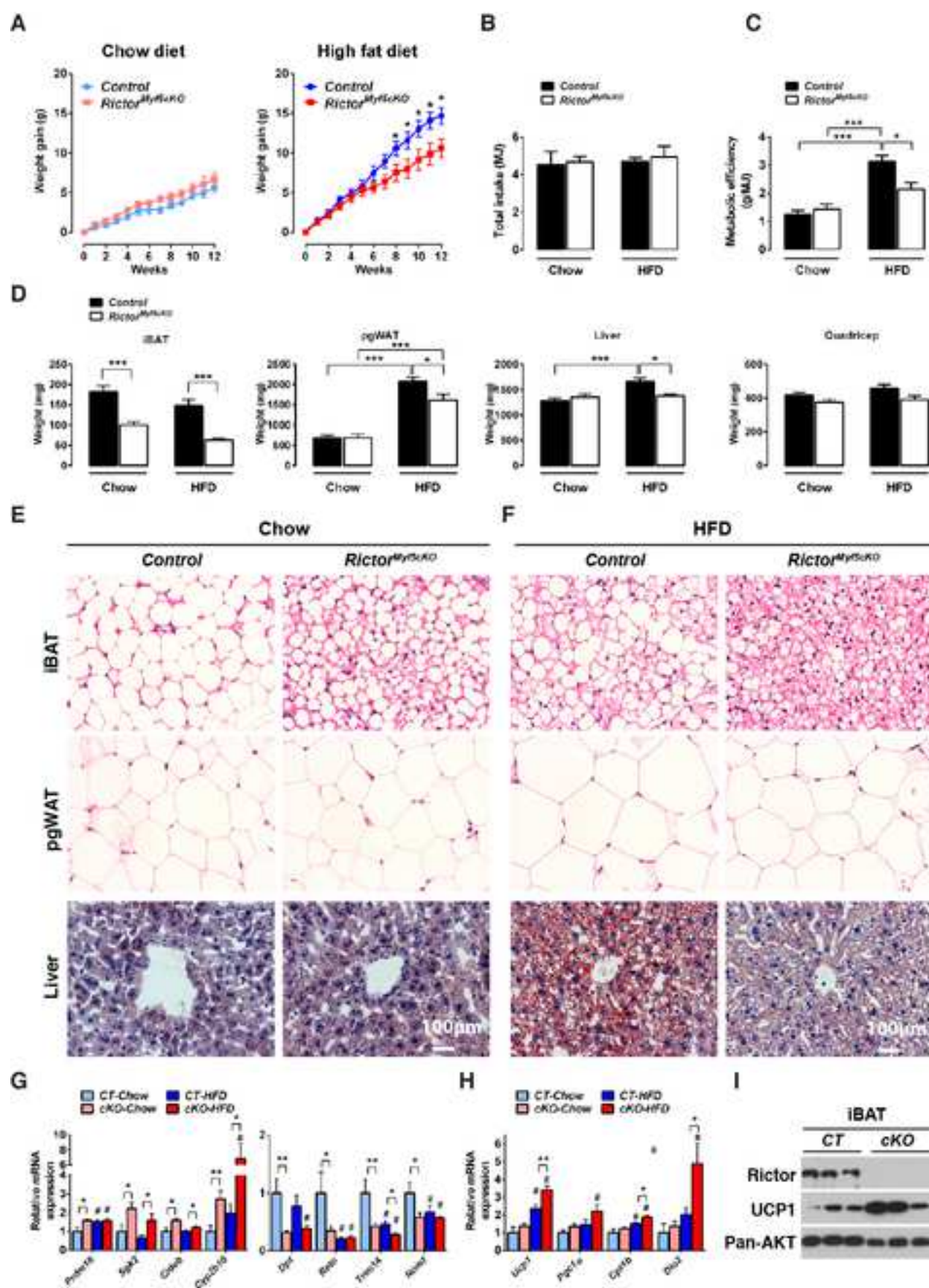


Figure 7
[Click here to download high resolution image](#)



Supplemental Information

Rictor/mTORC2 Loss in the *Myf5*-lineage Reprograms Brown Fat Metabolism and Protects Mice against Obesity and Metabolic Disease

Chien-Min Hung, Camila Martinez Calejman, Juan Sanchez-Gurmaches, Huawei Li, Clary B. Clish, Simone Hettmer, Amy J. Wagers, and David A. Guertin

Inventory of Supplemental Information

Figure S1, related to Figure 1

Figure S2, related to Figure 2

Figure S3, related to Figure 3

Figure S4, related to Figure 4

Figure S5, related to Figure 5

Figure S6, related to Figure 6

Figure S7, related to Figure 7

Supplemental Information

Rictor/mTORC2 Loss in the *Myf5*-lineage Reprograms Brown Fat Metabolism and Protects Mice against Obesity and Metabolic Disease

Chien-Min Hung, Camila Martinez Calejman, Juan Sanchez-Gurmaches, Huawei Li, Clary B. Clish, Simone Hettmer, Amy J. Wagers, and David A. Guertin

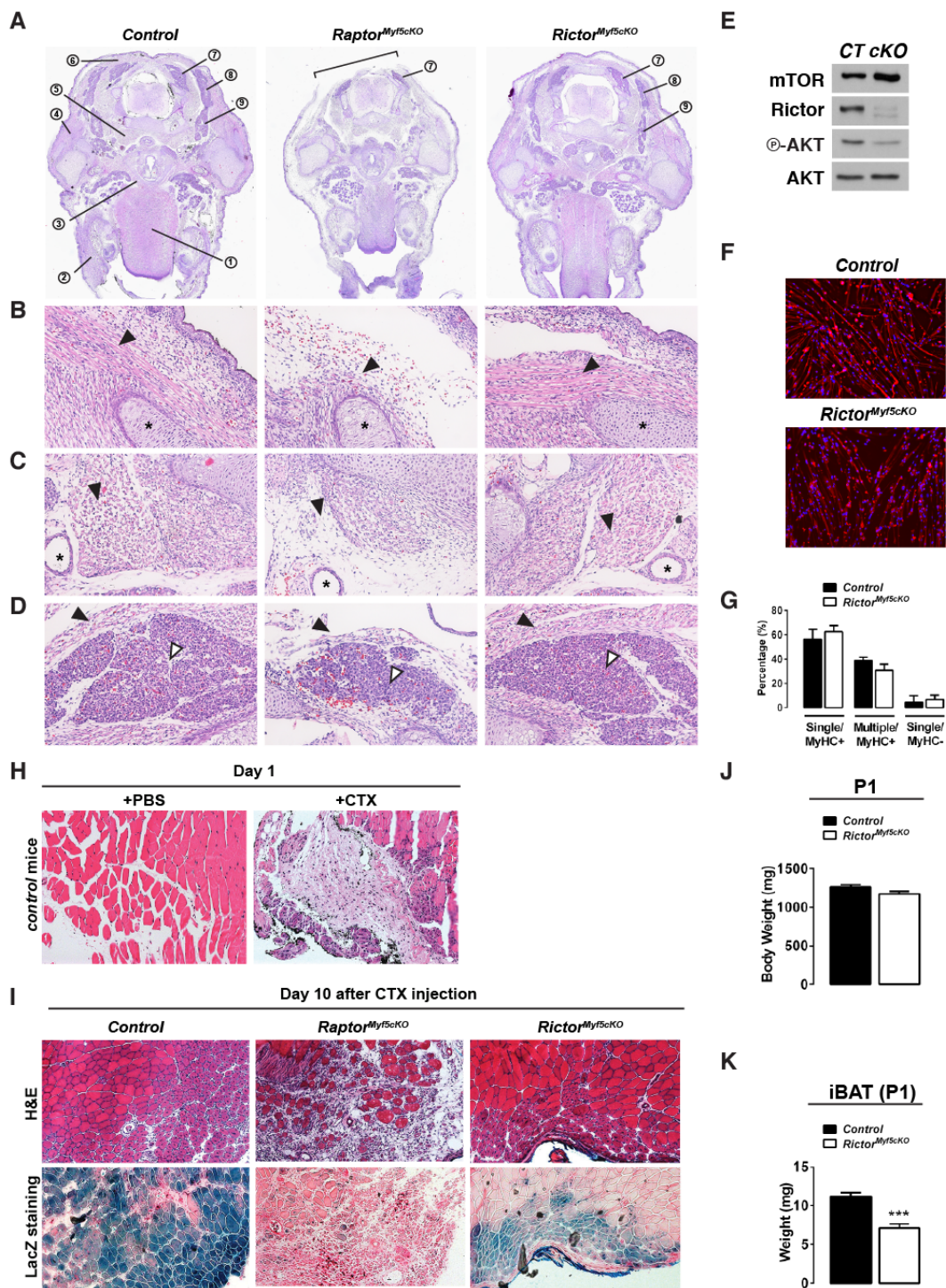


Figure S1, Related to Figure 1

(A) Transverse sections of E16.5 embryos. Tongue (1), masseter (2), sternohyoid and hyoglossus (3), supraspinatus (4), prevertebral (5), and trapezius muscles (7), and cervical BAT (7), interscapular BAT (8), and subscapular BAT precursors (9) are indicated. Bracket

marks region of hind neck fragility. **(B)** Enlarged image of supraspinatus muscle (arrowhead). Ossifying cartilage of the scapula marked with (*). **(C)** Enlarged image of prevertebral muscles of the neck (arrowhead). Carotid artery marked with (*). **(D)** Enlarged image of trapezius muscle (closed arrowhead) and cervical BAT precursors (open arrowhead). **(E)** Western blots of satellite cell lysates from control (*CT*) and *Rictor*^{*Myf5**ckO*} conditional knockout (*ckO*) mice. **(F)** Differentiated satellite cells stained with myosin heavy chain antibody. **(G)** Quantification of nuclei number in individual differentiated satellite cells. **(H)** H&E images of tibialis anterior (TA) muscle 1 day after PBS or cardiotoxin injection in control mice (see also supplementary methods). **(I)** Mice deleted for *Raptor* or *Rictor* specifically in satellite cells with *Pax7*-CreER were subjected to an acute cardiotoxin injury assay. Mice also carried the *Rosa26-LacZ* reporter to follow the deleted cells. H&E images and corresponding images for LacZ staining of TA muscle 10 days after cardiotoxin injection. Regenerated muscle cells in the control and *Rictor* KO are indicated by the centrally localized nuclei in H&E stained sections. No regenerated cells are detectable in the *Raptor* KO. **(J-K)** Total body weight (J) and average iBAT weight (K) at postnatal day 1 (n=6; bars represent mean ± SEM; t-test; ***p<0.001).

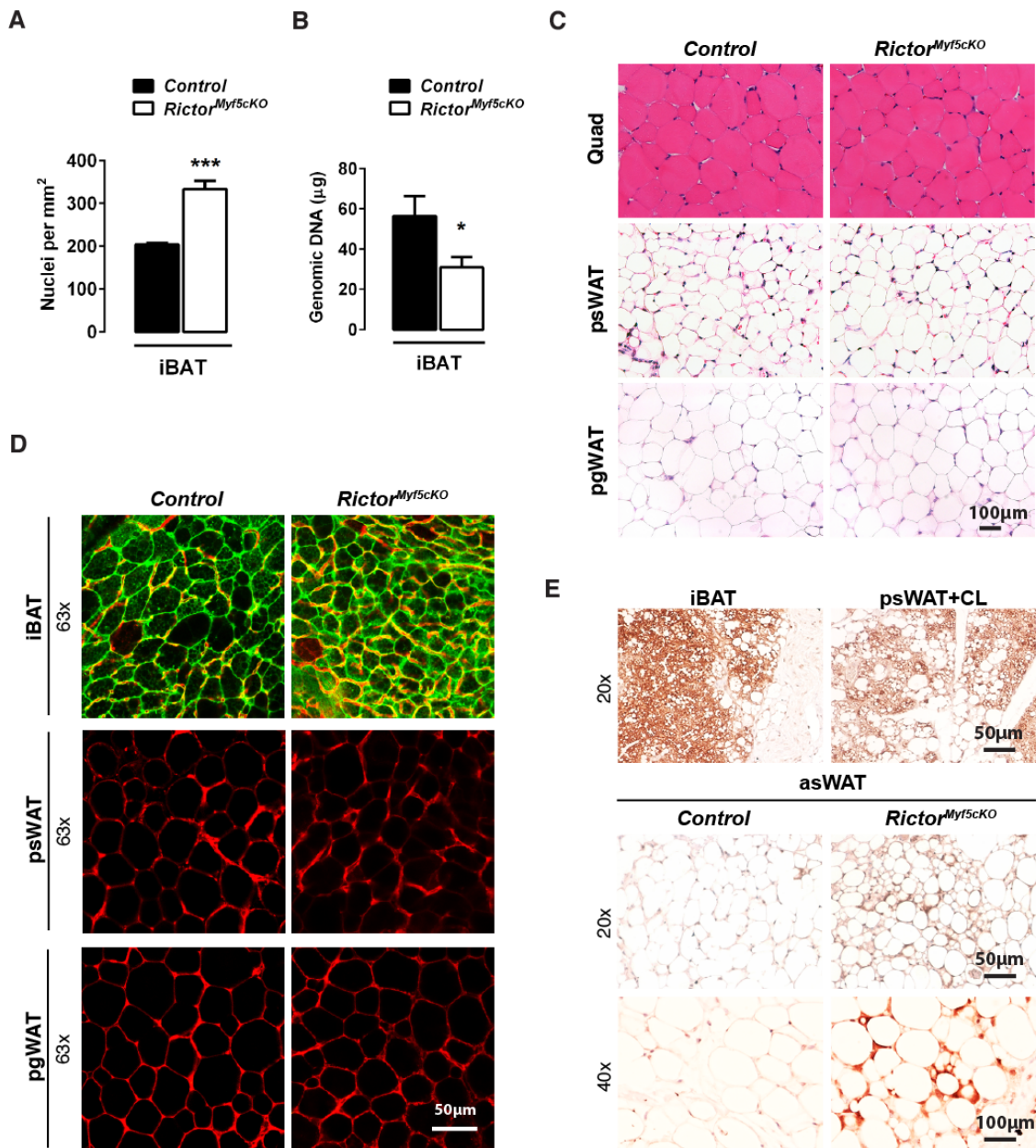


Figure S2, related to Figure 2.

(A) Nuclei density per mm² of iBAT (6-wks) (n=4; bars represent mean ± SEM; t-test; ***p<0.001). **(B)** Quantification of genomic DNA from iBAT (6-wks) (n=8; bars represent mean ± SEM; t-test; *p<0.05). **(C)** H&E stains (40x) of the quadriceps (Quad) muscle and posterior subcutaneous (psWAT) and perigonadal (pgWAT) white adipose tissue (6-wks). **(D)** Representative images of mTFP and mGFP labeled iBAT, psWAT and pgWAT adipocytes. Note adipocytes are homogeneously mGFP⁺ and smaller in the iBAT consistent with homogeneous *Rictor* loss in this tissue. **(E)** *Top*—UCP1 immunohistochemistry stains of iBAT and CL-316243 treated psWAT (20x). *Bottom*—asWAT (20x and 40x) from control and *Rictor^{Myf5cKO}* mice.

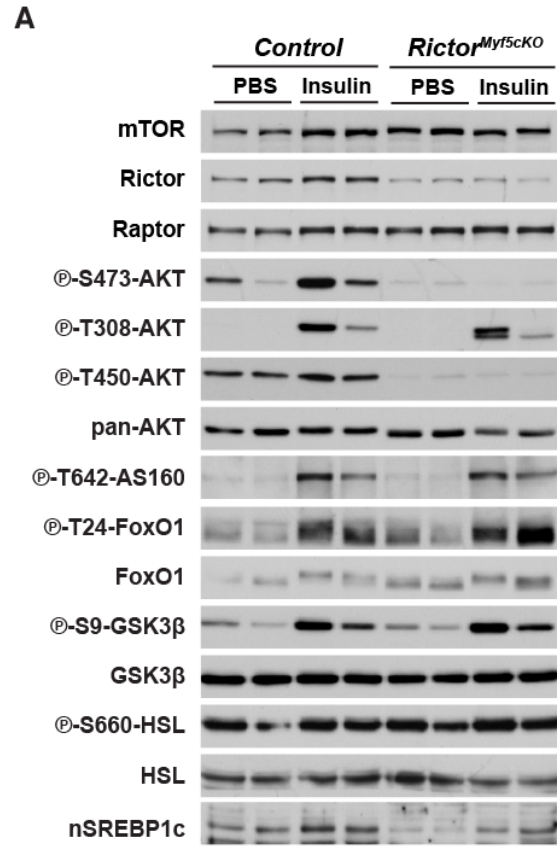
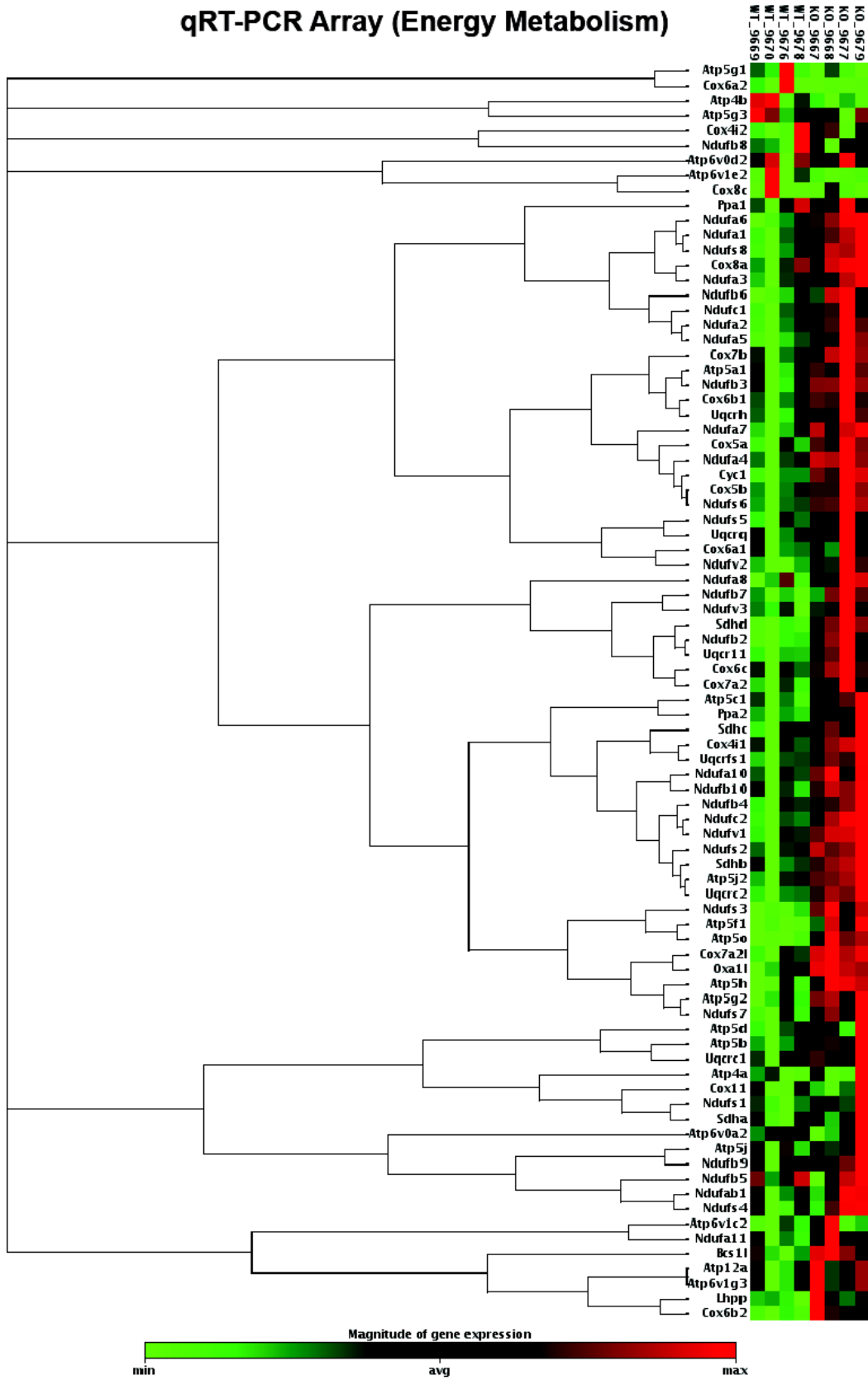


Figure S3, related to Figure 3.

(A) Western blots of the indicated total and phospho-proteins using lysates prepared from the iBAT of 8-week-old mice. Overnight fasted mice were *i.p.* injected with PBS or 150U/Kg insulin and tissues were collected 15 minutes post injection.

A

qRT-PCR Array (Energy Metabolism)



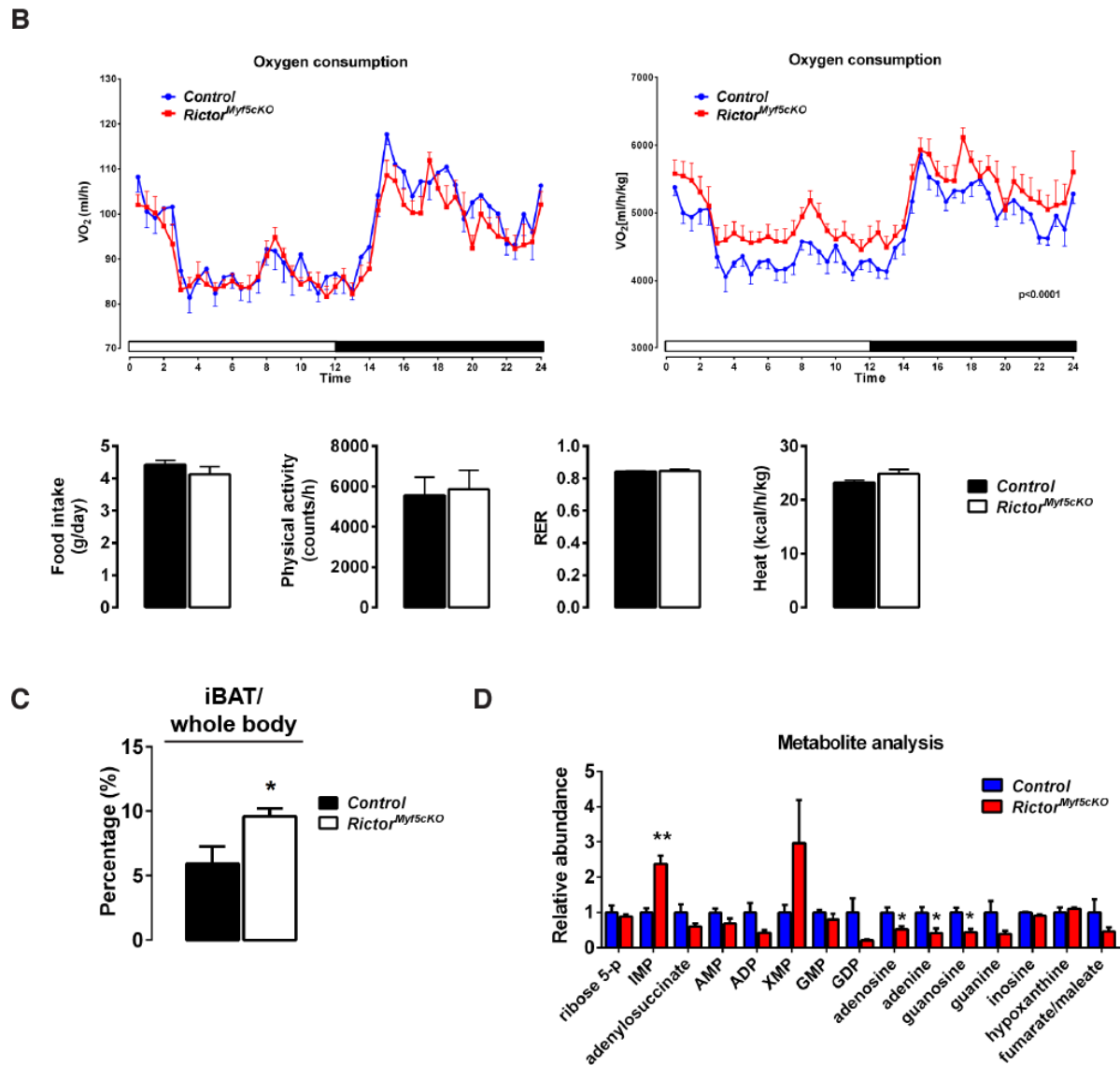


Figure S4, related to Figure 4.

(A) Clustering heat map for mitochondrial genes involved in energy metabolism qRT-PCR array (n=4). **(B)** Metabolic cage analysis of 6wk-old mice under normal housing temperature (22°C): *Top Left*—whole body oxygen consumption; *Top right*—whole body oxygen consumption normalized to body weight; *Bottom*—food intake, physical activity, respiratory exchange ratio (RER) and energy expenditure. (n=6) **(C)** Glucose uptake by ^{18}F FDG PET-CT (n=6; bars represent mean \pm SEM; t-test; *p<0.05). **(D)** Metabolite profiling was performed on 6-week control and *Rictor^{Myf5cKO}* iBAT. Note the high levels of IMP, a deamination product of AMP. AMP is formed by the adenylate kinase reaction, which produces ATP (2ADP = AMP + ATP). During metabolic stress or following treatment with chemical uncouplers, AMP is deaminated to IMP to ensure ongoing adenylate kinase activity and ATP production in order to maintain energy balance (Balcke et al., 2011).

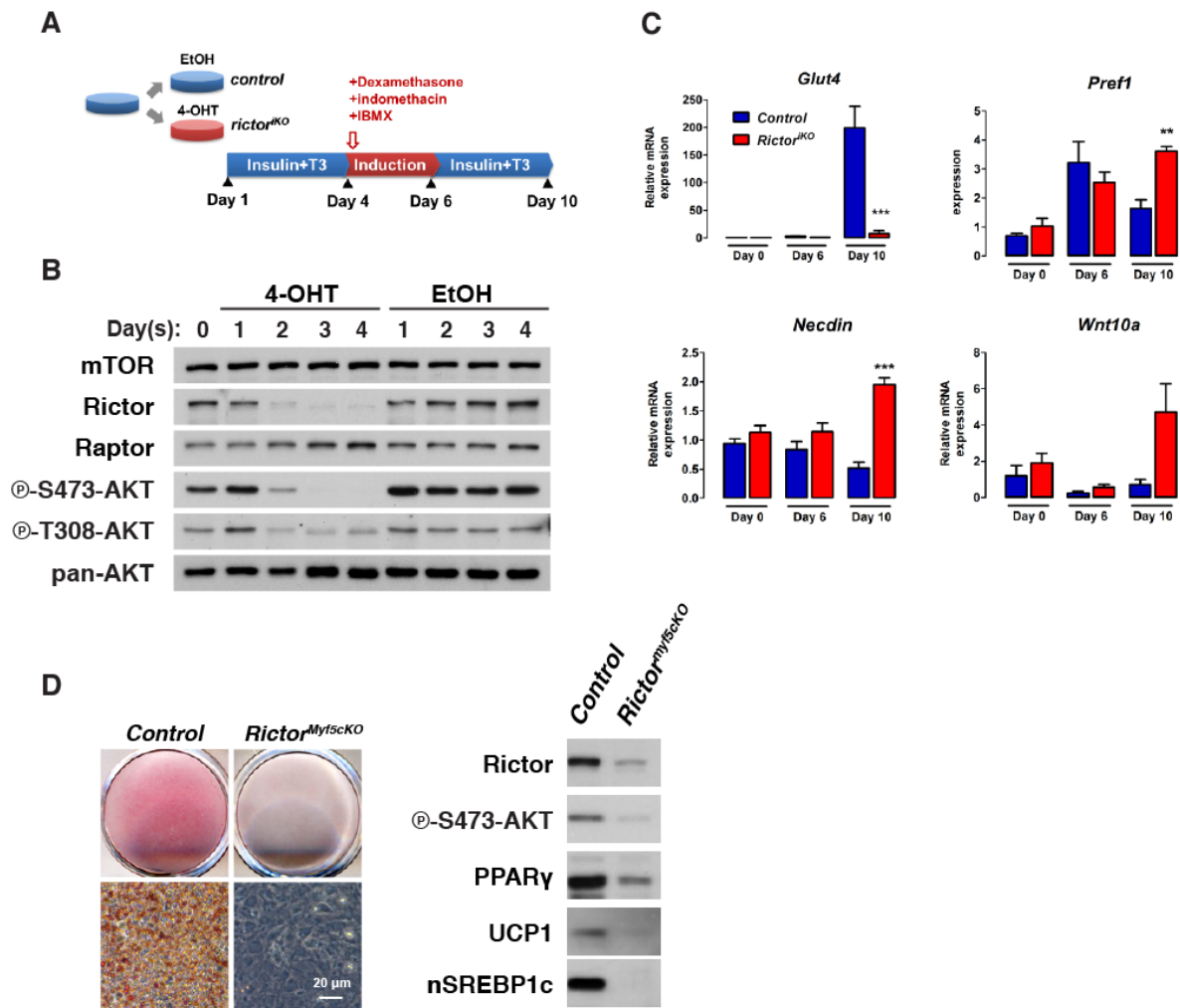


Figure S5, related to Figure 5.

(A) Inducible knockout differentiation protocol for comparing *Rictor^{IKO}* to isogenic control cells. Brown adipocyte precursors (bAPCs) were split from the same original dish into two dishes, one of which received vehicle (EtOH), the other 4-hydroxy-tamoxifen (4-OHT). After 3 days of treatment to induce deletion, cells were passed one time and then differentiated according to a standard 10-day brown adipocyte induction protocol (described in Experimental Procedures). **(B)** Western immunoblots showing time course following induced *Rictor* deletion in bAPCs with 4-OHT compared to vehicle (EtOH) treated isogenic controls. **(C)** qRT-PCR of mRNA levels for the indicated differentiation-related genes (n=3; bars represent mean \pm SEM; t-test; *p<0.05, ***p<0.001). **(D) Left**—Oil Red O staining of control and *Rictor^{Myf5cKO}* bAPCs after differentiation. **Right**—Western immunoblots showing indicated differentiation markers.

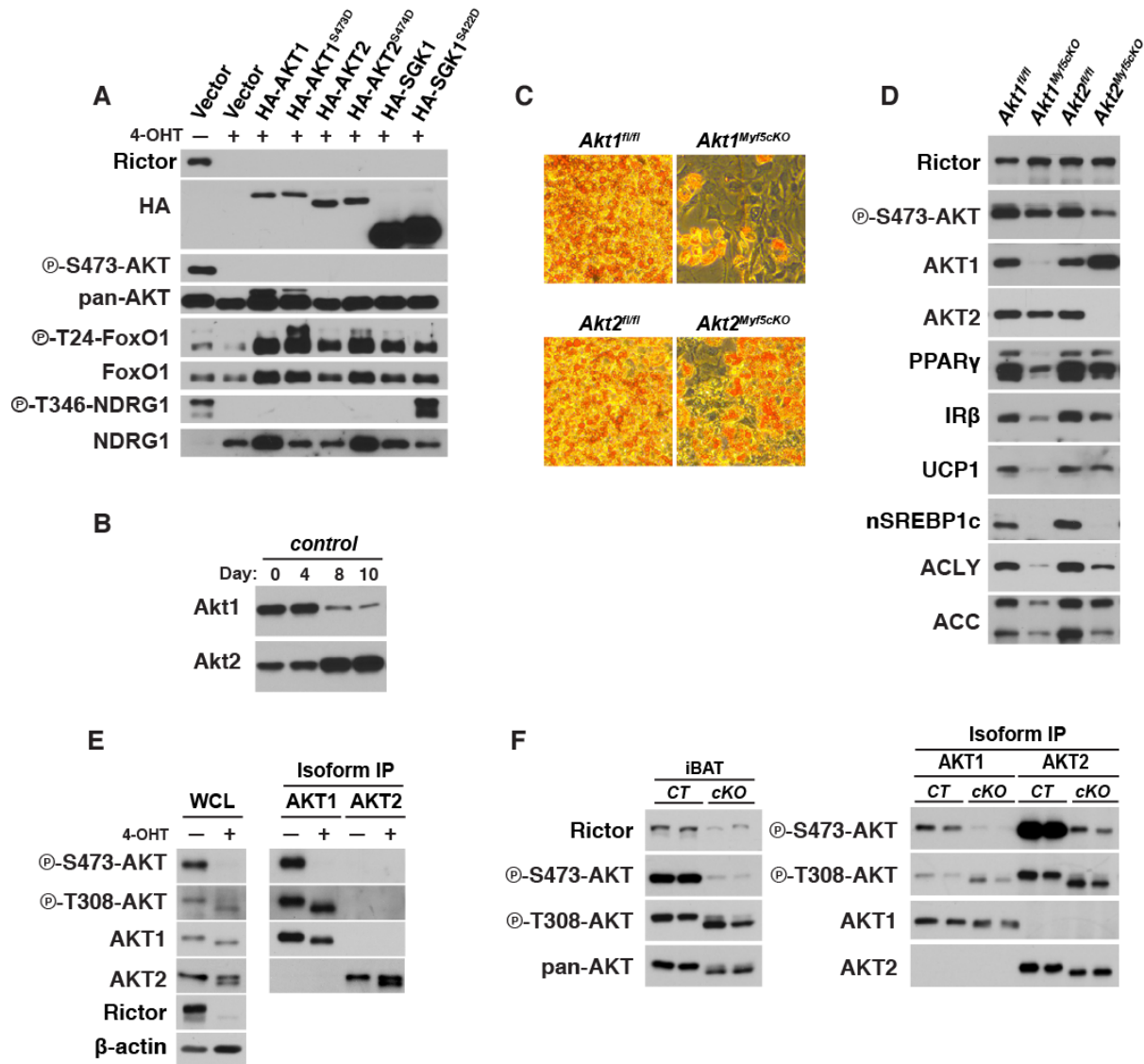


Figure S6, related to Figure 6.

(A) Western immunoblots of undifferentiated control and *Rictor^{iKO}* bAPCs stably expressing the indicated recombinant constructs. Cells were treated with fresh culture media before harvesting. **(B)** Western immunoblots of AKT1 and AKT2 protein expression at the indicated days during differentiation of wild type bAPCs. **(C)** Oil Red O staining of differentiated *Akt1* and *Akt2* conditional knockout and control bAPCs. The knockout cells were generated from *Myf5-cre;Akt1^{fl/fl}* or *Myf5-cre;Akt2^{fl/fl}* mice and the control cells are from their Cre-negative littermates. **(D)** Western immunoblots of lysates prepared from differentiated cells in (C). **(E)** Western immunoblots of lysates generated from AKT isoform-specific immunoprecipitation experiments using control or *Rictor^{iKO}* undifferentiated bAPCs. Immunoblots of the whole cell lysates (WCL) are shown to the left. **(F)** Western immunoblots of lysates generated from AKT isoform-specific immunoprecipitation experiments using iBAT dissected from 6-week-old control and *Rictor^{Myf5cKO}* mice.

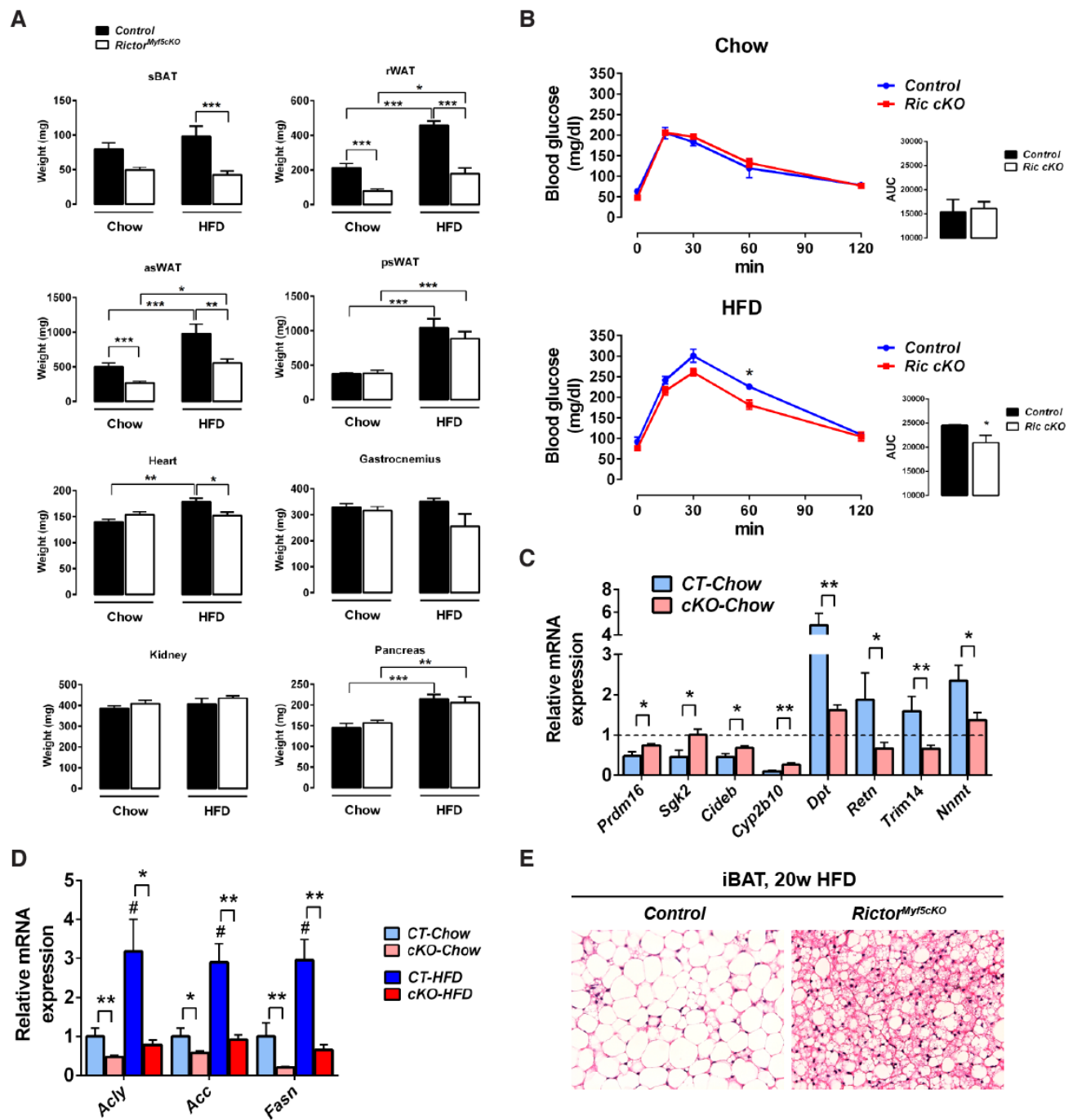


Figure S7, related to Figure 7.

(A) Mass (mg) of the indicated tissues collected from control and *Rictor^{Myf5cKO}* mice living at thermoneutrality (30°C) following 12-weeks of eating chow or HFD. (n=8 for control and n=12 for KO in chow; n=10 for both genotypes in HFD; bars represent mean \pm SEM; two-way ANOVA; *p<0.05, ***p<0.001) **(B)** Glucose tolerance test of control and *Rictor^{Myf5cKO}* mice on chow (top) or HFD (bottom) living at thermoneutrality. The test was performed

during the 11th week of the 12-week experiment. **(C)** qRT-PCR of the indicated brown and white fat genes in iBAT from control and *Rictor^{Myf5cKO}* mice eating chow diet and living at thermoneutrality (n=8 for control and n=12 for KO in chow; bars represent mean \pm SEM; two-way ANOVA; *p<0.05, **p<0.01, ***p<0.001). The expression level of each gene is normalized to the corresponding gene level in iBAT from age-matched control mice eating chow but living at the standard housing temperature (22°C). **(D)** qRT-PCR of the indicated lipogenesis genes in iBAT from chow or HFD mice (n=8 for control and n=12 for KO in chow; n=10 for both genotypes in HFD; bars represent mean \pm SEM; two-way ANOVA; *p<0.05, **p<0.01, ***p<0.001; # indicates significant difference over the control chow group). **(E)** Representative H&E images (n=4) of control and KO mice fed with HFD at thermoneutrality for 20 weeks.

Supplemental Experimental Procedures

Embryo analysis

Timed matings were performed and embryos were dissected at the indicated days. Embryos were fixed overnight in paraformaldehyde, paraffin embedded, and processed for histological analysis according to conventional methods.

Mice

Mice were kept on a daily 12 h light/dark cycle and fed a normal chow diet (Prolab® Isopro® RMH 3000) from LabDiet ad libitum at 22°C (except thermoneutrality studies). All animal experiments were approved by the University of Massachusetts Medical school animal care and use committee.

Satellite cells isolation and in vitro differentiation

Limb muscle including triceps surae (TS), tibialis anterior (TA), quadriceps and triceps were dissected and minced from 6 to 8-wks mice. Isolated interstitial and myofiber-associated cells were passed through 70µm nylon mesh and centrifuged at 1200 rpm. Red blood cells were removed from preparations by incubation with RBC lysis buffer (0.15 M ammonium chloride, 0.01 M potassium bicarbonate) on ice for 3 minutes. Antibody staining was performed for 20 min on ice in Hank's balanced salt solution supplemented with 2% FCS and 2 mM EDTA. After staining cells were filtered through a 35-µm cell-strainer capped tube to ensure single cell suspension. Sorting was performed immediately after filtration using a FACS Aria II cell sorter equipped with FASCDiva software. Cells were initially selected by size and shape and only live (PI-, calcein blue+) singlets were gated for further analysis of surface markers. Finally an enriched pool of cells (Sca-1-, Mac1-, Ter119-, CD45-, CXCR4+ and β1 integrin+) were purified and re-sorted with the same scheme described above to ensure the purity. Double sorted satellite cells were plated at 4×10^3 cells/well in collagen/laminin coated 96-well plates. Cells were maintained in growth media (20% horse serum in F10 media, Invitrogen) and feed with 5ng bovine FGF daily for 5 days. For inducing muscle fiber formation, cells were first transferred into matrigel (BD Bioscience)-coated chamber slides and grown in growth media with bFGF. 2~3

days later, cells were exposed to differentiation media (2% horse serum in F10 without bFGF). After 2 to 4 days myofiber can be observed and fixed with 4% paraformaldehyde. Myosin heavy chains and DAPI staining were performed as described in immunofluorescence section.

Muscle regeneration after cardiotoxin injury

To induce *Rictor* deletion in vivo, *Pax7-CreER^{T2}* mice were i.p. injected with 200µg/kg of tamoxifen (dissolved in ethanol first then diluted in corn oil to 10mg/mL) for consecutive 4 days. One day later the mice were anesthetized with 12mg/kg xylazine and 60mg/kg ketamine and 30µL cardiotoxin (10µmol/L from *Naja nigricollis*, Calbiochem) was directly injected into tibialis anterior muscle. 30µL PBS was given in contralateral TA muscle as control. 1 day and 10 days post injury, TA muscle was removed and muscle regeneration was examined by H&E staining and LacZ staining.

LacZ staining

Adipose tissue depots were fixed in 2% paraformaldehyde, 0.2% glutaraldehyde in PBS for 30 min at room temperature. The tissues were then washed 3 times for 15 min in wash buffer (PBS carrying 2 mM MgCl₂ and 0.02% Igepal® CA-630). Staining was performed in wash buffer containing X-gal (1mg/mL), potassium ferricyanide (5 mM) and potassium ferrocyanide (5 mM) at room temperature for at least 16 h. Next, tissues were further fixed in fixing solution for at least 12 h at room temperature, transferred to ethanol for dehydration, then sectioned at 5 µm thicknesses. Sections were counter-stained with nuclear fast red dehydrated and mounted using Citoseal™ 60 (Thermo Scientific). Lean tissues were snap frozen in isopentane-liquid nitrogen in OCT. Sections (10 µm) were stained overnight (X-gal (1mg/mL), potassium ferricyanide (5 mM) and potassium ferrocyanide (5 mM), MgCl₂ (2 mM) in PBS at 37°C and counter-stained with nuclear fast red, dehydrated and mounted.

Tissue harvest and histology

Adipose tissue depot notations are described in (Walden et al., 2011). Each tissue was carefully dissected to avoid contamination from surrounding tissue. Samples for RNA were

first immersed in RNAlater (Invitrogen) and stored at -80°C; otherwise, they were frozen down immediately in liquid nitrogen. For histology, tissue pieces were fixed by 10% formalin. Embedding, sectioning and Hematoxylin & Eosin (HE) staining was done by the UMass Morphology Core.

Immunohistochemistry

Adipose tissue sections were subjected to UCP1 IHC according to (Cohen et al., 2014). Briefly, fat sections were hydrated and antigen retrieval was done by incubating the sections in citrate buffer at 90-95°C water for 20 min. After blocking, primary antibody (anti-Ucp1 antibody, Abcam #ab10983) was applied overnight at 4°C. Next day, SuperPicture 3rd Gen IHC Detection Kit (Novex) was used for detection.

Whole-mount confocal microscopy

Indicated brown and white adipose tissues were dissected from 6 week-old mice and were mounted with Fluoromount-G (Southern Biotech) as described in (Berry and Rodeheffer, 2013). Mounted samples were imaged on a LSM 5 Pascal (Zeiss) point scanner confocal system. 40x objective was used with oil immersion. Background fluorescence was offset by using wild-type tissues (no *mT/mG* allele). GFP was excited at 488 nm and detected from 515 to 565 nm and iBAT from *Myf5-cre;Rosa26mT/mG* mice was used as positive control for GFP signal. TdTomato was excited at 543 nm and detected from 575 to 640 nm and pgWAT from *mT/mG* mice (without Cre-driver) was used as positive control for TdTomato.

Nuclei number and cell size quantification

ImageJ was used to quantify nuclei number in iBAT and cell size (diameter) in rWAT and asWAT. For each individual sample, 4 to 6 images were taken and analyzed. Nuclei density was presented as nuclei number per mm².

Genomic DNA quantification

Total genomic DNA was extracted and purified by using DNeasy Blood & Tissue kit (Qiagen) according to manufacturer's instruction. Isolated genomic DNA was quantified by NanoDrop 2000 (Thermo Scientific) spectrophotometer.

Immunofluorescence

Frozen section of interscapular brown adipose tissues were thawed and then fixed with methanol for 15 min at room temperature. The fixed sections were washed with 1mL PBS twice and then were permeabilized and blocked with PBSAT buffer (PBS with 1% BSA and 0.5% Triton X-100) for 15 min twice. Primary antibody against mitochondria Cox IV (1:100 dilution, CST #4850) was added to sections for overnight incubation. Slides were washed three times with 1mL PBSAT and incubated with secondary antibody conjugated with Alexa-568 or Alexa-647 (1:1000 dilution, Invitrogen) for 4 hours. Intensive wash was applied to remove unstained antibodies. DAPI was used to stain nuclei for 5 min and washed away by PBS immediately. The slides were embedded with 5 μ L mounting media (Prolong Gold, Invitrogen).

Glucose uptake

6-week old mice (n=5 per each genotype) were i.p. injected with ^{18}F -FDG, 364-483 uCi in 100 μ l saline, and 30 min later the PET imaging was performed in anesthetized animals (1.2-2% isoflurane carried in oxygen) immobilized on a Minerve bed (Bioscan). Immediately after PET acquisition, each mouse was transferred to the NanoSPECT/CT (Bioscan), for the CT acquisition. The PET images were reconstructed without photon attenuation correction using the PETView program (Philips) with the fully 3D iterative reconstruction algorithm, giving a pixel size of 1 mm. The CT acquisition was performed at standard frame resolution, 45 kVp tube voltage and 500 ms of exposure time. The CT reconstruction was accomplished using In-VivoScope 1.37 software (Bioscan). The PET image DICOM files were transferred to the NanoSPECT/CT reconstruction workstation to provide the PET/CT fusion images. Volume-of-Interest (VOI) analysis of the PET acquisitions was accomplished with the InVivo- Scope 1.37 software.

Transmission electron microscopy

iBATs (n=3 for each group) were dissected from 5 week-old mice and subjected to electron microscopy study done by Core Electron Microscopy Facility, UMass medical school.

Metabolite profiling

Brown fat samples were homogenized in four volumes of water using a TissueLyser II (Qiagen) and profiles of polar metabolites were obtained using LC-MS. The polar metabolite profiling methods were developed using reference standards of each metabolite to determine chromatographic retention times and MS multiple reaction monitoring transitions, declustering potentials and collision energies. The LC-MS methods have been recently described (Townsend et al., 2013). Briefly, negative ionization mode data were acquired using an ACQUITY UPLC (Waters) coupled to a 5500 QTRAP triple quadrupole mass spectrometer (AB SCIEX) running hydrophilic interaction chromatography (HILIC) method. A 30 μ L aliquot of each homogenate was extracted using 120 μ L of 80% methanol (VWR) containing 0.05 ng/ μ L inosine-15N4, 0.05 ng/ μ L thymine-d4, and 0.1 ng/ μ L glycocholate-d4 as internal standards (Cambridge Isotope Laboratories). The samples were centrifuged (10 min, 9,000 x g, 4°C) and the supernatants (10 μ L) were injected directly onto a 150 x 2.0 mm Luna NH2 column (Phenomenex) that was eluted at a flow rate of 400 μ L/min. Initial mobile phase conditions were 10% mobile phase A (20 mM ammonium acetate and 20 mM ammonium hydroxide (Sigma-Aldrich) in water (VWR)) and 90% mobile phase B (10 mM ammonium hydroxide in 75:25 v/v acetonitrile/methanol (VWR)) and the column was eluted using a 10 min linear gradient to 100% mobile phase A. The ion spray voltage was -4.5 kV and the source temperature was 500°C. Positive ionization mode data were acquired using an 1100 Series pump (Agilent) and an HTS PAL autosampler (Leap Technologies) coupled to a 4000 QTRAP triple quadrupole mass spectrometer (AB SCIEX). A 10 μ L aliquot of each homogenate was extracted using nine volumes of 74.9:24.9:0.2 (v/v/v) acetonitrile/methanol/formic acid containing stable isotope-labeled internal standards (0.2 ng/ μ L valine-d8, Isotec; and 0.2 ng/ μ L phenylalanine-d8 (Cambridge Isotope Laboratories)). Samples were centrifuged (10 min, 9,000 x g, 4°C) and supernatants (10 μ L) were injected onto a 150 x 2.1 mm Atlantis HILIC column (Waters).

The column was eluted isocratically at a flow rate of 250 $\mu\text{L}/\text{min}$ with 5% mobile phase A (10 mM ammonium formate and 0.1% formic acid in water) for 1 minute followed by a linear gradient to 40% mobile phase B (acetonitrile with 0.1% formic acid) over 10 minutes. The ion spray voltage was 4.5 kV and the source temperature was 450°C. MultiQuant 1.2 software (AB SCIEX) was used for automated peak integration and metabolite peaks were manually reviewed for quality of integration and compared against a known standard to confirm identity.

Cold challenge

Mice were first fasted for 16 hours and transferred into a 4°C cold room without any food in the cage. Rectal temperature was measured by rectal probe (RET-3, ThermoWorks) hourly for 6 hours. Mice were sacrificed and tissues were collected at the end of experiment. Fasted mice kept at 22°C were used as control for qRT-PCR.

Cell culture and retrovirus production

All cells were cultured in DMEM (Invitrogen) supplemented with 10% FBS and penicillin/streptomycin at a 37°C. Primary brown preadipocytes (bBPAs) were isolated from P1 neonates of *Ubc-creER^{T2};Rictor^{fl/fl}* mice, *Myf5-cre;Rictor^{fl/fl}*, *Myf5-cre;Akt1^{fl/fl}*, *Myf5-cre;Akt2^{fl/fl}* mice and control littermates according to (Fasshauer et al., 2001) and were immortalized with pBabe-SV40 Large T antigen and selected by puromycin resistance. For recombinant AKT and SGK construct expression, retroviruses were made by cotransfecting pBabe-puro plasmid harboring different *Akt* or *Sgk* cDNAs with pCL-Ampho in HEK-293T cells. 24h and 48h after transfection the viral supernatant was harvested and applied to MEFs for 12h. Cells stably expressing each construct were obtained after puromycin selection.

Differentiation

To generate *Rictor^{iKO}* cells *ubc-creER^{T2};Rictor^{fl/fl}* bAPCs were treated with two doses of 1 μM 4-OHT for 3 days. For brown preadipocyte differentiation, BPAs were seeded at 4x10⁴ cells/ml and allowed to proliferate to confluence over 3 days in differentiation media (20nM insulin, 1nM T₃). On the 4th day, cells were induced to differentiate by adding

induction media (20nM insulin, 1nM T₃, 0.125mM indomethacin, 2µg/mL dexamethasone and 0.5mM 3-isobutyl-1-methylxanthine (IBMX)) for 2 days; the medium was then changed every two days with fresh differentiation media until day 10. Differentiated bAPCs were fixed with PBS-buffered formalin and stained with Oil-Red-O dye.

Western blots

Cells were lysed in a buffer containing 50mM Hepes, pH 7.4, 40mM NaCl, 2mM EDTA, 1.5mM NaVO₄, 50mM NaF, 10mM sodium pyrophosphate, 10mM sodium β-glycerophosphate and 1% Triton X-100 typically 1 hour after the cells were replenished with fresh culture medium. Tissues were homogenized using a TissueLyser (Qiagen) in the same lysis buffer but additionally supplemented with 0.1% SDS, 1% sodium deoxycholate. An equal amount of total protein was loaded into acrylamide/bis-acrylamide gels and transferred to PVDF membranes for detection with the indicated antibodies. Briefly, membranes were incubated with primary antibodies in 5% milk/PBST or 5% BSA/PBST overnight. HRP-conjugated secondary antibodies were given for 1h. Western blots were developed by enhanced chemiluminescence (PerkinElmer) and detected by X-ray films.

Immunoprecipitation

AKT1-specific antibody (CST# 2967) and AKT2-specific antibody-conjugated beads (CST#4090) were used to purify each isoform. 500ug Cell lysates or tissue lysates were incubated with 1ul of antibodies at 4°C overnight. For AKT1 purification, protein-antibody complex was precipitated by 2 hrs incubation with protein G sepharose beads (Invitrogen). Samples were then boiled in 2x SDS sample buffer.

***Ex vivo* oxygen consumption**

Freshly isolated brown adipose tissues were rinsed with KHB buffer (111nM NaCl, 4.7mM KCl, 2mM MgSO₄, 1.2mM Na₂HPO₄, 0.5mM carnitine and 2.5mM glucose) and then cut into small pieces (5~10mg). After 5 times of washing with KHB buffer, each piece was placed into the center of one single well in a XF24 islet capture microplate (Seahorse Bioscience #101122-100) and covered by a provided screen. 450ul KHB buffer was loaded in each well and tissue

metabolic rates were measured following program: 3 cycles for basal oxygen consumption rate (OCR) (2 min mix, 2 min wait, and 3 min measure), then injection of 50ul 100mM pyruvate, then followed by 3 cycles for pyruvate-stimulated OCR (3 min mix, 3 min wait, and 2 min measure). Each OCR value was obtained from five different pieces of a tissue and from 3 repeated measurements. The final OCR values were the average of five independent experiments and normalized to genomic DNA content.

Gene expression analysis

Total RNA was isolated from cells or tissues using Qiazol (Invitrogen) and an RNeasy kit (Invitrogen). Equal amounts of RNA were retro-transcribed to cDNA using a High capacity cDNA reverse transcription kit (#4368813, Applied Biosystems). Quantitative RT-PCR was performed in 10 μ L reactions using a StepOnePlus real-time PCR machine from Applied Biosystems using SYBR Green PCR master mix (#4309156, Applied Biosystems) according to manufacturer instructions. Standard and melting curves were run in every plate for every gene to ensure efficiency and specificity of the reaction. *Tbp* expression was used as a normalization gene in all conventional RT-PCR experiments. Primer information is listed in the table below. Quantitative RT-PCR arrays for mitochondria (PAMM-087) and mitochondria energy metabolism (PAMM-008) were purchased from Qiagen. Interscapular brown fat pads were removed from 6-wks mice *ad libitum* and Rictor protein deletion in *Myf5-re;Rictor^{fl/fl}* samples was confirmed by western blots before analyzing expression. Data analysis was performed on web-based software provided by the manufacturer.

Primer sequences for quantitative RT-PCR analysis

| Gene | Forward primer (5'-3') | Reverse primer (5'-3') |
|-----------------------------------|------------------------|------------------------|
| <i>Tbp</i> | GAAGCTGCGGTACAATTCCAG | CCCCTTGTACCCTTCACCAAT |
| <i>Prdm16</i> | GACATTCCAATCCCACCAGA | CACCTCTGTATCCGTCAGCA |
| <i>Ppargc1α</i> | CCCTGCCATTGTTAAGACC | TGCTGCTGTTCTGTTTTTC |
| <i>Pparγ</i> | TCAGCTCTGTGGACCTCTCC | ACCCTTGCATCCTTCACAAG |
| <i>C/ebpα</i> | CAAGCCCAGCAACGAGTACCG | GTCACTGGTCAACTCCAGCAC |
| <i>C/ebpβ</i> | TCGGGACTTGATGCAATCC | AAACATCAACAACCCCGC |
| <i>C/ebpδ</i> | GCTTTGTGGTTGCTGTTGAA | ATCGACTTCAGCGCCTACA |

| | | |
|---|---------------------------|----------------------------|
| <i>Ucp1</i> | CTGCCAGGACAGTACCCAAG | TCAGCTGTTCAAAGCACACA |
| <i>DiO2</i> | TGCGCTGTGTCTGGAACAG | CTGGAATTGGGAGCATCTTCA |
| <i>Lpl</i> | GGCCAGATTCATCAACTGGAT | GCTCCAAGGCTGTACCCTAAG |
| <i>aP2</i> | GATGCCTTTGTGGGAACCT | CTGTCGTCTGCGGTGATTT |
| <i>Cidea</i> | ATCACAACCTGGCCTGGTTACG | TACTACCCGGTGTCCATTTCT |
| <i>Dpt</i> | CTGCCGCTATAGCAAGAGGT | TGGCTTGGGTACTCTGTTGTC |
| <i>Srebf1a</i> | TAGTCCGAAGCCGGGTGGGCGCCGG | GATGTCGTTCAAACCCGCTGTGTGTC |
| <i>Srebf1c</i> | AAGCAAATCACTGAAGGACCTGG | AAAGACAAGCTACTCTGGGAG |
| <i>Srebf2</i> | GGATCCTCCCAAAGAAGGAG | TTCCTCAGAACGCCAGACTT |
| <i>Chrebp</i> | CACTCAGGGAATACACGCCTAC | ATCTTGGTCTTAGGGTCTTCAGG |
| <i>Chrebpα</i> | CGACTCACCACCTCTTC | TTGTTCAGCCGGATCTTGTC |
| <i>Chrebpβ</i> | TCTGCAGATCGCGTGGAG | CTTGTCCCGGCATAGCAAC |
| <i>Acly</i> | CTCACACGGAAGCTCCATAA | ACGCCCTCATAGACACCATC |
| <i>Acc</i> | GGAGATGTACGCTGACCGAGAA | ACCCGACGCATGGTTTTCA |
| <i>Fasn</i> | GCTGCGGAAACTTCAGGAAAT | AGAGACGTGTCACTCCTGGACTT |
| <i>Elvol6</i> | TCAGCAAAGCACCCGAAC | AGCGACCATGTCTTTGTAGGAG |
| <i>Scd1</i> | CCCTGCGGATCTTCCTTATC | TGTGTTTCTGAGAACTTGTGGTG |
| <i>Insig1</i> | TGTGGTTCTCCAGGTGACT | TAGCCACCATCTTCTCCTCC |
| <i>Insig2</i> | TGAAGCAGACCAATGTTTCAA | GGTGAAGTGGGGGTCTCC |
| <i>Tfam</i> | GTCCATAGGCACCGTATTGC | CCCATGCTGGAAAAACACTT |
| <i>Cpt1b</i> | GGGCACCTCTGGGAGTTTGT | TTGGCTCACCCACACAGTGT |
| <i>Necdin</i> | CACTTCCTCTGCTGGTCTCC | ATCGCTGTCTGCATCTCAC |
| <i>Pref1</i> | AGTACGAATGCTCCTGCACAC | CTGGCCCTCATCATCCAC |
| <i>Wnt10a</i> | CACCCGGCCATACTTCT | CACTTACGCCGCATGTTCT |

*Primer sequences for the brown and white fat marker genes *Sgk2*, *Cideb*, *Cyp2b10*, *Retn*, *Trim14* and *Nnmt* are described in (Harms et al., 2014).

Supplemental References

Balcke, G.U., Kolle, S.N., Kamp, H., Bethan, B., Looser, R., Wagner, S., Landsiedel, R., and van Ravenzwaay, B. (2011). Linking energy metabolism to dysfunctions in mitochondrial respiration--a metabolomics in vitro approach. *Toxicology letters* 203, 200-209.

Berry, R., and Rodeheffer, M.S. (2013). Characterization of the adipocyte cellular lineage in vivo. *Nature cell biology* 15, 302-308.

Cohen, P., Levy, J.D., Zhang, Y., Frontini, A., Kolodin, D.P., Svensson, K.J., Lo, J.C., Zeng, X., Ye, L., Khandekar, M.J., Wu, J., Gunawardana, S.C., Banks, A.S., Camporez, J.P., Jurczak, M.J., Kajimura, S., Piston, D.W., Mathis, D., Cinti, S., Shulman, G.I., Seale, P., and Spiegelman, B.M. (2014). Ablation of PRDM16 and beige adipose causes metabolic dysfunction and a subcutaneous to visceral fat switch. *Cell* 156, 304-316.

Fasshauer, M., Klein, J., Kriauciunas, K.M., Ueki, K., Benito, M., and Kahn, C.R. (2001). Essential role of insulin receptor substrate 1 in differentiation of brown adipocytes. *Molecular and cellular biology* 21, 319-329.

Harms, M.J., Ishibashi, J., Wang, W., Lim, H.W., Goyama, S., Sato, T., Kurokawa, M., Won, K.J., and Seale, P. (2014). Prdm16 is required for the maintenance of brown adipocyte identity and function in adult mice. *Cell metabolism* 19, 593-604.

Townsend, M.K., Clish, C.B., Kraft, P., Wu, C., Souza, A.L., Deik, A.A., Tworoger, S.S., and Wolpin, B.M. (2013). Reproducibility of Metabolomic Profiles among Men and Women in 2 Large Cohort Studies. *Clinical chemistry* 59, 1657-1667.

Walden, T.B., Hansen, I.R., Timmons, J.A., Cannon, B., and Nedergaard, J. (2011). Recruited versus nonrecruited molecular signatures of brown, "brite" and white adipose tissues. *Am J Physiol Endocrinol Metab.*